REVIEW ARTICLE

Optical trapping

Keir C. Neuman and Steven M. Block[a]
Department of Biological Sciences, and Department of Applied Physics, Stanford University, Stanford, California 94305

Since their invention just over 20 years ago, optical traps have emerged as a powerful tool with broad-reaching applications in biology and physics. Capabilities have evolved from simple manipulation to the application of calibrated forces on—and the measurement of nanometer-level displacements of—optically trapped objects. We review progress in the development of optical trapping apparatus, including instrument design considerations, position detection schemes and calibration techniques, with an emphasis on recent advances. We conclude with a brief summary of innovative optical trapping configurations and applications.
© *2004 American Institute of Physics.* [DOI: 10.1063/1.1785844]

I. INTRODUCTION

Arthur Ashkin pioneered the field of laser-based optical trapping in the early 1970s. In a series of seminal papers, he demonstrated that optical forces could displace and levitate micron-sized dielectric particles in both water and air,[1] and he developed a stable, three-dimensional trap based on counterpropagating laser beams.[2] This seminal work eventually led to the development of the single-beam gradient force optical trap,[3] or "optical tweezers," as it has come to be known.[4] Ashkin and co-workers employed optical trapping in a wide-ranging series of experiments from the cooling and trapping of neutral atoms[5] to manipulating live bacteria and viruses.[6,7] Today, optical traps continue to find applications in both physics and biology. For a recent survey of the literature on optical tweezers see Ref. 8. The ability to apply picoNewton-level forces to micron-sized particles while simultaneously measuring displacement with nanometer-level precision (or better) is now routinely applied to the study of molecular motors at the single-molecule level,[9–19] the physics of colloids and mesoscopic systems,[20–29] and the mechanical properties of polymers and biopolymers.[18,20,30–43] In parallel with the widespread use of optical trapping, theoretical and experimental work on fundamental aspects of optical trapping is being actively pursued.[4,20,44–48] In addition to the many excellent reviews of optical trapping[9,49–53] and specialized applications of optical traps, several comprehensive guides for building optical traps are now available.[54–60] For the purpose of this review, we will concentrate on the fundamental aspects of optical trapping with particular emphasis on recent advances.

Just as the early work on optical trapping was made possible by advances in laser technology,[4] much of the recent progress in optical trapping can be attributed to further technological development. The advent of commercially available, three-dimensional (3D) piezoelectric stages with capacitive sensors has afforded unprecedented control of the position of a trapped object. Incorporation of such stages into optical trapping instruments has resulted in higher spatial precision and improved calibration of both forces and displacements. In addition, stage-based force clamping techniques have been developed that can confer certain advantages over other approaches of maintaining the force, such as dynamically adjusting the position or stiffness of the optical trap. The use of high-bandwidth position detectors[61] improves force calibration, particularly for very stiff traps, and extends the detection bandwidth of optical trapping measurements. In parallel with these technological improvements, recent theoretical work has led to a better understanding of 3D position detection[62–64] and progress has been made in calculating the optical forces on spherical objects with a range of sizes.[65,66]

II. PRINCIPLES OF OPTICAL TRAPPING

An optical trap is formed by tightly focusing a laser beam with an objective lens of high numerical aperture (NA). A dielectric particle near the focus will experience a force due to the transfer of momentum from the scattering of incident photons. The resulting optical force has traditionally been decomposed into two components: (1) a scattering force, in the direction of light propagation and (2) a gradient force, in the direction of the spatial light gradient. This decomposition is merely a convenient and intuitive means of discussing the overall optical force. Following tradition, we present the optical force in terms of these two components, but we stress that both components arise from the very same underlying physics (see theoretical progress, below for a unified expression). The scattering component of the force is the more familiar of the two, which can be thought of as a photon "fire hose" pushing the bead in the direction of light propagation. Incident light impinges on the particle from one direction, but is scattered in a variety of directions, while some of the incident light may be absorbed. As a result, there

[a] Electronic mail: sblock@stanford.edu

is a net momentum transfer to the particle from the incident photons. For an isotropic scatter, the resulting forces cancel in all but the forward direction, and an effective scattering cross section can be calculated for the object. For most conventional situations, the scattering force dominates. However, if there is a steep intensity gradient (i.e., near the focus of a laser), the second component of the optical force, the gradient force, must be considered. The gradient force, as the name suggests, arises from the fact that a dipole in an inhomogeneous electric field experiences a force in the direction of the field gradient.[67] In an optical trap, the laser induces fluctuating dipoles in the dielectric particle, and it is the interaction of these dipoles with the inhomogeneous electric field at the focus that gives rise to the gradient trapping force. The gradient force is proportional to both the polarizability of the dielectric and the optical intensity gradient at the focus.

For stable trapping in all three dimensions, the axial gradient component of the force pulling the particle towards the focal region must exceed the scattering component of the force pushing it away from that region. This condition necessitates a very steep gradient in the light, produced by sharply focusing the trapping laser beam to a diffraction-limited spot using an objective of high NA. As a result of this balance between the gradient force and the scattering force, the axial equilibrium position of a trapped particle is located slightly beyond (i.e., down-beam from) the focal point. For small displacements ($\sim$150 nm), the gradient restoring force is simply proportional to the offset from the equilibrium position, i.e., the optical trap acts as Hookean spring whose characteristic stiffness is proportional to the light intensity.

In developing a theoretical treatment of optical trapping, there are two limiting cases for which the force on a sphere can be readily calculated. When the trapped sphere is much larger than the wavelength of the trapping laser, i.e., the radius $(a) \gg \lambda$, the conditions for Mie scattering are satisfied, and optical forces can be computed from simple ray optics (Fig. 1). Refraction of the incident light by the sphere corresponds to a change in the momentum carried by the light. By Newton's third law, an equal and opposite momentum change is imparted to the sphere. The force on the sphere, given by the rate of momentum change, is proportional to the light intensity. When the index of refraction of the particle is greater than that of the surrounding medium, the optical force arising from refraction is in the direction of the intensity gradient. Conversely, for an index lower than that of the medium, the force is in the opposite direction of the intensity gradient. The scattering component of the force arises from both the absorption and specular reflection by the trapped object. In the case of a uniform sphere, optical forces can be directly calculated in the ray-optics regime.[68,69] The extremal rays contribute disproportionally to the axial gradient force, whereas the central rays are primarily responsible for the scattering force. Thus, expanding a Gaussian laser beam to slightly overfill the objective entrance pupil can increase the ratio of trapping to scattering force, resulting in improved trapping efficiency.[69,70] In practice, the beam is typically expanded such that the $1/e^2$ intensity points match the objective aperture, resulting in $\sim$87% of the incident power entering the objective. Care should be exercised when overfilling the objective. Absorption of the excess light by the blocking aperture can cause heating and thermal expansion of the objective, resulting in comparatively large ($\sim\mu$m) axial motions when the intensity is changed. Axial trapping efficiency can also be improved through the use of "donut" mode trapping beams, such as the TEM_{01}^* mode or Laguerre-Gaussian beams, which have intensity minima on the optical propagation axis.[69,71–73]
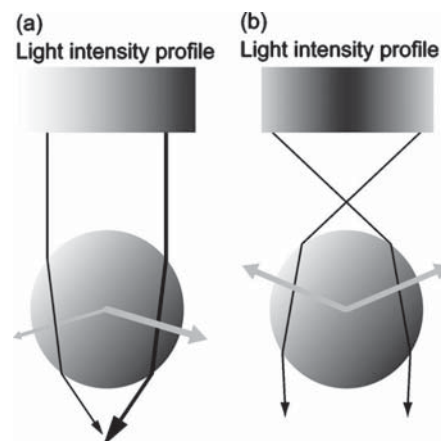

FIG. 1. Ray optics description of the gradient force. (A) A transparent bead is illuminated by a parallel beam of light with an intensity gradient increasing from left to right. Two representative rays of light of different intensities (represented by black lines of different thickness) from the beam are shown. The refraction of the rays by the bead changes the momentum of the photons, equal to the change in the direction of the input and output rays. Conservation of momentum dictates that the momentum of the bead changes by an equal but opposite amount, which results in the forces depicted by gray arrows. The net force on the bead is to the right, in the direction of the intensity gradient, and slightly down. (B) To form a stable trap, the light must be focused, producing a three-dimensional intensity gradient. In this case, the bead is illuminated by a focused beam of light with a radial intensity gradient. Two representative rays are again refracted by the bead but the change in momentum in this instance leads to a net force towards the focus. Gray arrows represent the forces. The lateral forces balance each other out and the axial force is balanced by the scattering force (not shown), which decreases away from the focus. If the bead moves in the focused beam, the imbalance of optical forces will draw it back to the equilibrium position.

When the trapped sphere is much smaller than the wavelength of the trapping laser, i.e., $a \ll \lambda$, the conditions for Raleigh scattering are satisfied and optical forces can be calculated by treating the particle as a point dipole. In this approximation, the scattering and gradient force components are readily separated. The scattering force is due to absorption and reradiation of light by the dipole. For a sphere of radius a, this force is

$$F_{\text{scatt}} = \frac{I_0 \sigma n_m}{c}, \tag{1}$$

$$\sigma = \frac{128 \pi^5 a^6}{3 \lambda^4} \left(\frac{m^2 - 1}{m^2 + 2} \right)^2, \tag{2}$$

where I_0 is the intensity of the incident light, σ is the scattering cross section of the sphere, n_m is the index of refraction of the medium, c is the speed of light in vacuum, m is the ratio of the index of refraction of the particle to the index of the medium (n_p/n_m), and λ is the wavelength of the trap-

ping laser. The scattering force is in the direction of propagation of the incident light and is proportional the intensity. The time-averaged gradient force arises from the interaction of the induced dipole with the inhomogeneous field

$$F_{\text{grad}} = \frac{2\pi\alpha}{cn_m^2} \nabla I_0, \qquad (3)$$

where

$$\alpha = n_m^2 a^3 \left(\frac{m^2 - 1}{m^2 + 2} \right) \qquad (4)$$

is the polarizability of the sphere. The gradient force is proportional to the intensity gradient, and points up the gradient when $m > 1$.

When the dimensions of the trapped particle are comparable to the wavelength of the trapping laser ($a \sim \lambda$), neither the ray optic nor the point-dipole approach is valid. Instead, more complete electromagnetic theories are required to supply an accurate description.[74–80] Unfortunately, the majority of objects that are useful or interesting to trap, in practice, tend to fall into this intermediate size range ($0.1-10\lambda$). As a practical matter, it can be difficult to work with objects smaller than can be readily observed by video microscopy ($\sim 0.1 \ \mu$m), although particles as small as ~ 35 nm in diameter have been successfully trapped. Dielectric microspheres used alone or as handles to manipulate other objects are typically in the range of $\sim 0.2-5 \ \mu$m, which is the same size range as biological specimens that can be trapped directly, e.g., bacteria, yeast, and organelles of larger cells. Whereas some theoretical progress in calculating the force on a sphere in this intermediate size range has been made recently,[65,66] the more general description does not provide further insight into the physics of optical trapping. For this reason we postpone discussion of recent theoretical work until the end of the review.

III. DESIGN CONSIDERATIONS

Implementing a basic optical trap is a relatively straightforward exercise (Fig. 2).[55,58] The essential elements are a trapping laser, beam expansion and steering optics, a high NA objective, a trapping chamber holder, and some means of observing the trapped specimen. Optical traps are most often built by modifying an inverted microscope so that a laser beam can be introduced into the optical path before the objective: the microscope then provides the imaging, trapping chamber manipulation, and objective focus functions. For anything beyond simply trapping and manually manipulating objects, however, additional elements become necessary. Dynamic control of trap position and stiffness can be achieved through beam steering and amplitude modulation elements incorporated in the optical path before the laser beam enters the objective. Dynamic control over position and stiffness of the optical trap has been exploited to implement position- and force-clamp systems. Position clamps, in which the position of a trapped object is held constant by varying the force, are well suited for stall force measurements of molecular motors.[39,49,81–83] Force clamps, in which the force on a trapped object is fixed by varying the position of the trap, are
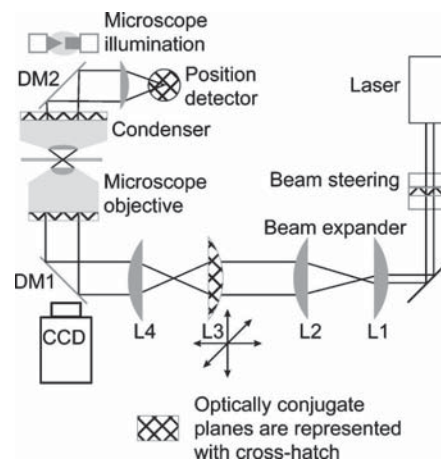

FIG. 2. Layout of a generic optical trap. The laser output beam usually requires expansion to overfill the back aperture of the objective. For a Gaussian beam, the beam waist is chosen to roughly match the objective back aperture. A simple Keplerian telescope is sufficient to expand the beam (lenses $L1$ and $L2$). A second telescope, typically in a 1:1 configuration, is used for manually steering the position of the optical trap in the specimen plane. If the telescope is built such that the second lens, $L4$, images the first lens, $L3$, onto the back aperture of the objective, then movement of $L3$ moves the optical trap in the specimen plane with minimal perturbation of the beam. Because lens $L3$ is optically conjugate (conjugate planes are indicated by a cross-hatched fill) to the back aperture of the objective, motion of $L3$ rotates the beam at the aperture, which results in translation in the specimen plane with minimal beam clipping. If lens $L3$ is not conjugate to the back aperture, then translating it leads to a combination of rotation *and* translation at the aperture, thereby clipping the beam. Additionally, changing the spacing between $L3$ and $L4$ changes the divergence of the light that enters the objective, and the axial location of the laser focus. Thus, $L3$ provides manual three-dimensional control over the trap position. The laser light is coupled into the objective by means of a dichroic mirror ($DM1$), which reflects the laser wavelength, while transmitting the illumination wavelength. The laser beam is brought to a focus by the objective, forming the optical trap. For back focal plane position detection, the position detector is placed in a conjugate plane of the condenser back aperture (condenser iris plane). Forward scattered light is collected by the condenser and coupled onto the position detector by a second dichroic mirror ($DM2$). Trapped objects are imaged with the objective onto a camera. Dynamic control over the trap position is achieved by placing beam-steering optics in a conjugate plane to the objective back aperture, analogous to the placement of the trap steering lens. For the case of beam-steering optics, the point about which the beam is rotated should be imaged onto the back aperture of the objective.

well suited for displacement measurements.[49,56,81,84,85] Incorporation of a piezoelectric stage affords dynamic positioning of the sample chamber relative to the trap, and greatly facilitates calibration. Furthermore, for the commonly employed geometry in which the molecule of interest is attached between the surface of the trapping cell and a trapped bead "handle," piezoelectric stages can be used to generate a force clamp.[86–88] The measurement of force and displacement within the optical trap requires a position detector, and, in some configurations, a second, low power laser for detection. We consider each of these elements in detail.

A. Commercial systems

Commercial optical trapping systems with some limited capabilities are available. Cell Robotics[89] manufactures a laser-trapping module that can be added to a number of inverted microscopes. The module consists of a 1.5 W diode pumped Nd:YVO$_4$ laser ($\lambda=1064$ nm) with electronic inten-

sity control, and all of the optics needed to both couple the laser into the microscope and manually control the position of the trap in the specimen plane. The same module is incorporated into the optical tweezers workstation, which includes a microscope, a motorized stage and objective focus, video imaging, and a computer interface. Arryx Incorporated[90] manufactures a complete optical trapping workstation that includes a 2 W diode pumped solid-state laser ($\lambda=532$ nm), holographic beam shaping and steering, an inverted microscope, a motorized stage, and computer control. Holographic beam shaping provides control over the phase of the trapping laser,[91,92] which allows multiple, individually addressable, optical traps in addition to high order, complex trapping beams. An integrated optical trap is also available from PALM Microlaser Technologies,[93] either alone or incorporated with their microdissection system. The PALM system employs an infrared trapping laser and computer control of the stage, similar to the other optical trapping systems. The commercial systems tend to be expensive, but they offer turnkey convenience at the price of flexibility and control. None of the systems currently comes equipped with position detection capabilities beyond video imaging, and only one (Arryx) provides dynamic control over the trap position, but with an unknown update rate (~5 Hz or less). Overall, these systems are adequate for positioning and manipulating objects but are incapable, without further modifications, of ultrasensitive position or force measurements. As commercial systems become increasingly sophisticated and versatile, they may eventually offer an "off-the-shelf" option for some optical trapping applications. In deciding between a commercial or custom-built optical trap, or among commercial systems, several factors should be considered. Basic considerations include cost, maximum trap force and stiffness, choice of laser wavelength (important for biological samples), specimen or trap positioning capability, optical imaging modes, position-detection capabilities, and sample geometry. In addition, flexibility and the possibility to upgrade or improve aspects of the system should also be considered. How easily can the optical system be modified or adapted? Can the functionality be upgraded? Perhaps the most fundamental question concerns the decision to buy or to build. Whereas building a basic optical trap is now standard practice in many labs, it requires a certain familiarity with optics and optical components (in relation to the complexity of the optical trap), as well as a significant time investment for the design, construction, and debugging phases. These factors should be weighed against the potential benefits of reduced cost, increased flexibility and greater control of home-built optical traps.

B. Trapping laser

The basic requirement of a trapping laser is that it delivers a single mode output (typically, Gaussian TEM$_{00}$ mode) with excellent pointing stability and low power fluctuations. A Gaussian mode focuses to the smallest diameter beam waist and will therefore produce the most efficient, harmonic trap. Pointing instabilities lead to unwanted displacements of the optical trap position in the specimen plane, whereas power fluctuations lead to temporal variations in the optical
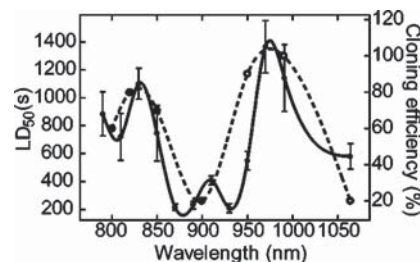

FIG. 3. The wavelength dependence of photodamage in *E. coli* compared to Chinese hamster ovary (CHO) cells. (Solid circles and solid line, left axis, half lethal dose time for *E. coli* cells (LD$_{50}$); open circles and dashed line, right axis, cloning efficiency in CHO cells determined by Liang *et al.* (Ref. 96) (used with permission). Lines represent cubic spline fits to the data). The cloning efficiency in CHO cells was determined after 5 min of trapping at 88 mW in the specimen plane (error bars unavailable), selected to closely match to our experimental conditions (100 mW in the specimen plane, errors shown as ± standard error in the mean). Optical damage is minimized at 830 and 970 nm for both *E. coli* and CHO cells, whereas it is most severe in the region between 870 and 930 nm (reprinted from Ref. 95).

trap stiffness. Pointing instability can be remedied by coupling the trapping laser to the optical trap via an optical fiber, or by imaging the effective pivot point of the laser pointing instability into the front focal plane of the objective. Both of these solutions however, trade reduced pointing stability against additional amplitude fluctuations, as the fiber coupling and the clipping by the back aperture of the microscope objective depend on beam pointing. Thus, both power and pointing fluctuations introduce unwanted noise into any trapping system. The choice of a suitable trapping laser therefore depends on several interdependent figures of merit (power, power stability, pointing stability, thermal drift, wavelength, mode quality, etc.).

Output power of the trapping laser and the throughput of the optical system will determine the maximum attainable stiffness and force. As discussed above, trapping forces depend on multiple parameters and are difficult to calculate for most conditions of practical interest. Generally speaking, maximum trapping forces on the order of 1 pN per 10 mW of power delivered to the specimen plane can be achieved with micron-scale beads.[9] As a specific example, trapping a 0.5 μm polystyrene ($n=1.57$) sphere in water with a TEM$_{00}$ 1064 nm laser that overfills a 1.2 NA objective by ~10% ($1/e^2$ intensity points matched to the aperture radius), gives a stiffness of 0.16 pN/nm per W of power in the specimen plane. In practice, laser power levels can range from a few mW to a Watt or more in the specimen plane, depending on details of the laser and setup, objective transmittance, and the desired stiffness.

Wavelength is an important consideration when biological material is trapped, particularly for *in vivo* trapping of cells or small organisms.[94] There is a window of relative transparency in the near infrared portion of the spectrum (~750–1200 nm), located in the region between the absorption of proteins in the visible and the increasing absorption of water towards the infrared.[9] Substantial variation with wavelength of optical damage to biological specimens is observed even within the near infrared region (Fig. 3), with damage minima occurring at 970 and 830 nm[95–97] for bacterial cells of *Escherichia coli*. If dam-

age or "opticution"[98] of biological specimens is not a concern, then the choice of wavelength becomes less critical, but the potential effects of heating resulting from light absorption by the medium or the trapped particle should certainly be considered.[99–101] The optimal choice of trapping wavelength will also depend on the transmission of the objective used for optical trapping (discussed below), as well as the output power available at a given wavelength.

In practice, a variety of lasers has been employed for optical trapping. The factors discussed above, along with the cost, will determine the final selection of a trapping laser. The laser of choice for working with biological samples is currently the neodymium:yttrium–aluminum–garnet (Nd:YAG) laser and its close cousins, neodymium:yttrium–lithium–fluoride (Nd:YLF), and neodymium:yttrium–orthovanadate (Nd:YVO$_4$). These lasers operate in the near infrared region of the spectrum at 1.047, 1.053, or 1.064 μm, which helps to limit optical damage. Diode pumped versions of these lasers offer high power (up to 10 W or even more) and superior amplitude and pointing stability. An additional advantage of diode-pumped solid-state (DPSS) lasers is that the noise and heat of the laser power supply can be physically isolated from the laser itself and the immediate region of the optical trap. The output of the pump diodes can be delivered to the laser head via an optical fiber bundle, in some cases up to 10 m in length. The main drawback of such DPSS lasers is their cost, currently on the order of \$5–10 K per W of output power. Diode lasers afford a lower-cost alternative in a compact package and are available at several wavelengths in the near infrared, but these devices are typically limited to less than ~250 mW in a single-transverse mode, the mode required for efficient trapping. Diode lasers also suffer significantly from mode instabilities and noncircular beams, which necessitates precise temperature control instrumentation and additional corrective optics. By far the most expensive laser option is a tunable cw titanium:sapphire (Ti:sapphire) laser pumped by a DPSS laser, a system that delivers high power (~1 W) over a large portion of the near infrared spectrum (~750–950 nm), but at a current cost in excess of \$100 K. The large tuning range is useful for parametric studies of optical trapping, to optimize the trapping wavelength, or to investigate the wavelength-dependence of optical damage.[95] A Ti:sapphire laser is also employed for optical trapping *in vivo*[94] since it is the only laser currently available that can deliver over ~250 mW at the most benign wavelengths (830 and 970 nm).[95]

In optical trapping applications where no biological materials will be trapped, any laser source that meets the basic criteria of adequate power in the specimen plane, sufficient pointing and amplitude stability, and a Gaussian intensity profile, may be suitable. Optical traps have been built based on argon ion,[3] helium-neon,[102] and diode laser sources,[103,104] to name a few. The DPSS lasers employed in our lab for biological work supply ~4 W of power at 1064 nm with power fluctuations below 1%–2% and a long-term pointing stability of ±50 μrad.

C. Microscope

Most optical traps are built around a conventional light microscope, requiring only minor modifications. This approach reduces the construction of an optical trap to that of coupling the light from a suitable trapping laser into the optical path before the objective without compromising the original imaging capabilities of the microscope. In practice, this is most often achieved by inserting a dichroic mirror, which reflects the trapping laser light into the optical path of the microscope but transmits the light used for microscope illumination. Inverted, rather than upright, microscopes are often preferred for optical trapping because their stage is fixed and the objective moves, making it easier to couple the trapping light stably. The use of a conventional microscope also makes it easier to use a variety of available imaging modalities, such as differential interference contrast and epifluorescence.

With more extensive modifications, a position detector can be incorporated into the trapping system. This involves adding a second dichroic mirror on the condenser side of the microscope, which reflects the laser light while transmitting the illuminating light. In order to achieve the mechanical stability and rigidity required for nanometer scale position measurements, more extensive modifications of the microscope are generally required.[50,59] In the current generation of optical traps, the rotating, multiobjective turret is conventionally replaced with a custom-built single objective holder, along with a mount for the dichroic mirror. The original stage is removed and the microscope is modified to accommodate a more substantial stage platform, holding a crossed-roller bearing stage (for coarse movement) mounted to a piezoelectric stage with feedback (for fine movement). Finally, the condenser assembly is attached to a fine focus transport (similar to that used for the objective) that is then mounted to the illumination column by a rigid aluminum beam.[59]

An alternative to the redesign and retrofitting of a commercial microscope is to build the entire optical trap from individual optical components.[57,103,104] This approach is slightly more involved, as the entirety of the imaging and trapping optical paths have to be designed and built. The increase in complexity, however, can be offset by increased flexibility in the design and a wider choice of components, greater access to the optical paths, and reduced cost.

D. Objective

The single most important element of an optical trap is the objective used to focus the trapping laser. The choice of objective determines the overall efficiency of the optical trapping system (stiffness versus input power), which is a function of both the NA and the transmittance of the objective. Additionally, the working distance and the immersion medium of the objective (oil, water, or glycerol) will set practical limits on the depth to which objects can be trapped. Spherical aberrations, which degrade trap performance, are proportional to the refractive index mismatch between the immersion medium and the aqueous trapping medium. The deleterious effect of these aberrations increases with focal depth. The working distance of most high NA oil immersion
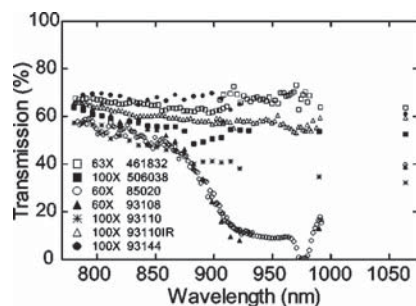
FIG. 4. Microscope objective transmission curves. Transmission measurements were made by means of the dual-objective method. Part numbers are cross-referenced in Table I. The uncertainty associated with a measurement at any wavelength is ~5% (reprinted from Ref. 95).

objectives is quite short (~0.1 mm), and the large refractive index mismatch between the immersion oil ($n = 1.512$) and the aqueous trapping medium ($n \sim 1.32$) leads to significant spherical aberrations. In practice, this limits the maximum axial range of the optical trap to somewhere between 5 and 20 μm from the coverglass surface of the trapping chamber.[104] Trapping deeper into solution can be achieved with water immersion objectives that minimize spherical aberration[105] and which are available with longer working distances. A high NA objective (typically, 1.2–1.4 NA) is required to produce an intensity gradient sufficient to overcome the scattering force and produce a stable optical trap for microscopic objects, such as polystyrene beads. The vast majority of high NA objectives are complex, multielement optical assemblies specifically designed for imaging visible light, not for focusing an infrared laser beam. For this reason, the optical properties of different objectives can vary widely over the near infrared region (Fig. 4).[9,95] Generally speaking, objectives designed for general fluorescence microscopy display superior transmission over the near infrared compared to most general-purpose objectives, as do infrared-rated objectives specifically produced for use with visible and near infrared light (Table I). Given the wide variation in transmission characteristics for different objectives, an objective being considered for optical trapping should be characterized at the wavelength of the trapping light. Manufacturers rarely supply the transmission characteristics of objectives outside the visible portion of the spectrum. When transmission characteristics in the near infrared are provided, the figures may represent an overestimate, since the throughput of the objective is often measured using an integrating sphere, which

also registers scattered light that is not well focused, and hence does not contribute to trapping. To measure the effective transmission of a high NA objective accurately, the dual objective method is preferred,[9,95,106] in which two identical, matched objectives are used to focus and then recollimate the laser beam (the transmission of a single objective is the square root of the transmission for the objective pair). Furthermore, because the transmission may depend on the degree to which light is bent, the laser beam should be expanded to fill the objective rear aperture. It should be noted that the extremely steep focusing produced by high NA objectives can lead to specular reflection from surfaces at the specimen plane, so simply measuring the throughput of an objective by placing the probe of a power meter directly in front of the objective lens results in an underestimation of its transmission. This approach is not recommended.

E. Position detection

Sensitive position detection lies at the heart of quantitative optical trapping, since nanoscale measurements of both force and displacement rely on a well-calibrated system for determining position. Position tracking of irregularly shaped objects is feasible, but precise position *and force calibration* are currently only practical with spherical objects. For this purpose, microscopic beads are either used alone, or attached to objects of interest as "handles," to apply calibrated forces. The position detection schemes presented here were primarily developed to track microscopic silica or polystyrene beads. However, the same techniques may be applied to track other objects, such as bacterial cells.[107–109]

1. Video based position detection

For simple imaging of a trapped particle, a video camera mounted to the camera port of the microscope (or elsewhere) often suffices. By digitally processing the signal acquired from the camera, and knowing the size subtended by a single pixel (e.g., by calibrating the video picture against a distance standard, such as a ruled objective micrometer), the position of a trapped object can be determined with subpixel accuracy (typically, to within ~5 nm or better), using any of several centroid-finding algorithms.[110–112] Video tracking of trapped objects using such algorithms has been implemented in real time,[113,114] but this approach is restricted to video acquisition rates (typically ~25–120 Hz), and the precision is ultimately limited by video timing jitter (associated with frame

TABLE I. Transmission of microscope objectives, cross-referenced with Fig. 2.

Part No.	Manufacturer	Magnification/ Tube length (mm)/ Numerical aperture	Type designation	Transmission (±5%)			
				830 (nm)	850 (nm)	990 (nm)	1064 (nm)
461832	Zeiss	63/160/1.2 Water	Plan NeoFluar	66	65	64	64
506038	Leica	100/∞/1.4-0.7 Oil	Plan Apo	58	56	54	53
85020	Nikon	60/160/1.4 Oil	Plan Apo	54	51	17	40
93108	Nikon	60/∞/1.4 Oil	Plan Apo CFI	59	54	13	39
93110	Nikon	100/∞/1.4 Oil	Plan Apo CFI	50	47	35	32
93110IR	Nikon	100/∞/1.4 Oil	Plan Apo IR CFI	61	60	59	59
93144	Nikon	100/∞/1.3 Oil	Plan Fluor CFI	67	68	—	61

acquisition) or variations in illumination. In principle, temporal resolution could be improved through the use of high speed video cameras. Burst frame rates in excess of 40 kHz can be achieved with specialized complementary metal oxide semiconductor (CMOS) cameras, for example. However, the usefulness of high speed cameras can be limited by computer speed or memory capacity. Current CPU speed limits real-time position tracking to ~500 Hz,[115] while practical storage considerations limit the number of high-resolution frames that can be stored to ~10^5, which corresponds to less than 2 min of high-speed video at 1 kHz. Even if these technological hurdles are overcome, high-speed video tracking is ultimately limited by the number of recorded photons (since shorter exposures require more illumination), so spatial resolution decreases as the frame rate increases. Generally speaking, the signal-to-noise ratio is expected to decrease as the square root of the frame rate. The discrepancy between the low video bandwidth (~100 Hz) and the much higher intrinsic bandwidth of even a relatively weak optical trap (~kHz) results in aliasing artifacts, and these preclude the implementation of many of the most effective calibration methods. Furthermore, video-based methods are not well suited to the measurement of the *relative* position of an object with respect to the trap center, further complicating force determination.

2. Imaging position detector

Several alternative (nonvideo) methods have been developed that offer precise, high-bandwidth position detection of trapped objects. The simplest of these is to image directly the trapped object onto a quadrant photodiode (QPD).[56,116,117] The diode quadrants are then summed pairwise, and differential signals are derived from the pairs for both x and y dimensions. If desired, the differential signals can be normalized by the sum signal from the four quadrants to reduce the dependence of the output on the total light intensity. Direct imaging of a trapped particle is typically restricted to a small zone within the specimen plane, and requires careful coalignment of the trap with the region viewed by the detector. Moreover, the high magnification required to achieve good spatial resolution results in comparatively low light levels at the QPD, ultimately limiting bandwidth and noise performance.[49,50] The latter limitation has been addressed by the use of a diode laser operating just below its lasing threshold, acting as a superbright, incoherent illumination source.[56] Imaging using laser illumination is considered impractical because of the speckle and interference that arise from coherent illumination over an extended region. Various laser phase-randomization approaches may relieve this restriction, but these typically carry additional disadvantages, most often reduced temporal bandwidth.

3. Laser-based position detection

Laser-based position detection is appealing, because it is possible to use a single laser for both trapping and position detection. Unlike the imaging detector scheme described above, laser-based detection requires the incorporation of a dichroic mirror on the condenser side of the microscope to couple out the laser light scattered by the specimen. Further-

more, the detector and its associated optics (lens, filters) must be stably mounted on (or next to) the condenser to collect the output light. Two different laser-based position detection schemes have been developed. The first relies on polarization interferometry.[9,49,50,118,119] This method is quite analogous to differential interference contrast (DIC) microscopy, and it relies on a subset of the DIC imaging components within the microscope. Incoming plane polarized laser light is split by a Wollaston prism into two orthogonal polarizations that are physically displaced from one another. After passing through the specimen plane, the beams are recombined in a second Wollaston prism and the polarization state of the recombined light is measured. A simple polarimeter consists of a quarter wave plate (adjusted so that plane-polarized light is transformed into circularly polarized light) followed by a polarizing beam splitter. The intensity in each branch of the beam splitter is recorded by a photodiode, and the normalized differential diode signal supplies the polarization state of the light. A bead centered in the trap introduces an equal phase delay in both beams, and the recombined light is therefore plane polarized. When the bead is displaced from its equilibrium position, it introduces a relative phase delay between the two beams, leading to a slight elliptical polarization after the beams are recombined. The ellipticity of the recombined light can be calibrated against physical displacement by moving a bead a known distance through the optical trap. This technique is extraordinarily sensitive[118] and is, in theory, independent of the position of the trapped object within the specimen plane, because the trapping and detection laser beams are one and the same, and therefore intrinsically aligned. In practice, however, there is a limited range over which the position signal is truly independent of the trap position. A further limitation of this technique is that it is one dimensional: it is sensitive to displacement along the Wollaston shear axis, providing position detection in a single lateral direction.

A second type of laser-based position detection scheme—back focal plane detection—relies on the interference between forward-scattered light from the bead and unscattered light.[59,64,120–122] The interference signal is monitored with a QPD positioned along the optical axis at a plane conjugate to the back focal plane of the condenser (rather than at an imaging plane conjugate to the specimen). The light pattern impinging on the QPD is then converted to a normalized differential output in both lateral dimensions as described above. By imaging the back focal plane of the condenser, the position signal becomes insensitive to absolute bead position in the specimen plane, and sensitive instead to the relative displacement of the bead from the laser beam axis.[120] As with the polarization interferometer, the detection beam and the optical trap are intrinsically aligned, however the QPD detection scheme can supply position information in both lateral dimensions.

Laser-based position detection schemes have also been implemented with a second, low-power detection laser.[49,50,59,81] The experimental complication of having to combine, spatially overlap, and then separate the trapping and detection beams is frequently outweighed by the advantages conferred by having an independent detection laser.

Uncoupling trapping and detection may become necessary, for example, when there are multiple traps produced in the specimen plane, or if the absolute position of a bead is the relevant measure, rather than the relative position of a bead from the optical trap. When dynamic position control of the optical trap is implemented (see below), a separate detection laser permits rapid position calibration of each trapped particle, and greatly simplifies position measurements in situations in which the trap is being moved.[50] The choice of a laser for position sensing is less constrained than that of a trapping laser, and only a few mW of output power suffice for most detection schemes. The total power should be kept as low as feasible to prevent the detection light from generating significant optical forces itself, thereby perturbing the trap. A detection laser wavelength chosen to match the peak sensitivity of the photodetector will minimize the amount of power required in the specimen plane. Separating the detection and trapping wavelengths facilitates combining and separating the two beams, but increases the constraints on the dichroic mirror that couples the laser beams into the microscope. We have found that combining two beams of similar wavelength is most easily accomplished with a polarizing beamsplitter, i.e., the beams are orthogonally plane polarized and combined in the polarizer before entering the microscope. Since the trapping and detection wavelengths are closely spaced, a single reflection band on the coupling dichroic mirror suffices to couple both beams into and out of the microscope. A holographic notch filter in front of the position detector provides ~6 orders of magnitude of rejection at the trapping wavelength, permitting isolation and measurement of the much less intense detection beam.

4. Axial position detection

The detection schemes described above were developed to measure lateral displacement of objects within the specimen plane, a major focus of most optical trapping work. Detecting axial motion within the optical trap has rarely been implemented and has not been as well characterized until recently. Axial motion has been determined by: measuring the intensity of scattered laser light on an overfilled photodiode;[123–126] through two-photon fluorescence generated by the trapping laser;[127–130] and by evanescent-wave fluorescence at the surface of a coverglass.[131,132] Although these various approaches all supply a signal related to axial position, they require the integration of additional detectors and, in some cases, fluorescence capability, into the optical trapping instrument. This can be somewhat cumbersome, consequently the techniques have not been widely adopted. The axial position of a trapped particle can also be determined from the total laser intensity in the back focal plane of the condenser.[62,64] The axial position signal derives from the interference between light scattered by the trapped particle and the unscattered beam. On passing through a focus, the laser light accumulates a phase shift of π, known as the Gouy phase.[133] The axial phase shift is given by $\psi(z) = \tan^{-1}(z/z_0)$, where z_0 is the Rayleigh range ($z_0 = \pi w_0^2/\lambda$, where w_0 is the beam waist and λ is the wavelength of light), and z is the axial displacement from the focus.[133] Light scattered by a particle located near the focus will preserve the

phase that it acquired prior to being scattered, whereas unscattered light will accumulate the full Gouy phase shift of π. The far-field interference between the scattered and unscattered light gives rise to an axial position-dependent intensity, which can be measured, for example, at the back focal plane of the condenser (see below and Fig. 8). This is the axial counterpart, in fact, of the lateral interference signal described above. Axial position detection can be achieved through a simple variant of quadrant photodiode-based lateral position detection. Recording the total incident intensity on the position detector supplies the axial position of trapped particle relative to the laser focus.[63,64] In contrast to lateral position detection, axial position detection is inversely proportional to the NA of the detector.[62,63] When a single detector is used to measure both lateral and axial position simultaneously, an intermediate detector NA should be used to obtain reasonable sensitivity in all three dimensions.

5. Detector bandwidth limitations

Position detection based on lasers facilitates high bandwidth recording because of the high intensity of light incident on the photodetector. However, the optical absorption of silicon decreases significantly beyond ~850 nm, therefore position sensing by silicon-based photodetectors is intrinsically bandwidth limited in the near infrared.[61,134] Berg-Sørenson and co-workers[134] demonstrated that the electrical response of a typical silicon photodiode to infrared light consists of both a fast and a slow component. The fast component results from optical absorption in the depletion region of the diode, where the optically generated electron hole pairs are rapidly swept to the electrodes. This represents the intended behavior of the diode, and is valid at wavelengths that are readily absorbed by the active material, i.e., $\lambda < \sim 1 \ \mu m$. At longer wavelengths, however, a slow component also appears in the diode response, due to absorption of light beyond the depletion region. Electron–hole pairs generated in this zone must diffuse into the depletion region before flowing on to the electrodes, a much slower process. Infrared light is poorly absorbed by silicon, resulting in a greater proportion of the incident light being absorbed beyond the depletion region, increasing the relative contribution of the slow component. Thus, the output of the diode effectively becomes lowpass filtered ($f_{3dB} \sim 8-9$ kHz at 1064 nm) in an intensity-, wavelength-, and reverse bias-dependent manner.[134] In principle, the effect of this lowpass filtering could be calculated and compensated, but in practice, this approach is complicated by the intensity dependence of the parasitic filtering. One workaround would be to employ a detection laser at a wavelength closer to the absorption maximum of silicon, i.e., shorter than ~850 nm. Two other solutions include using nonsilicon-based detectors employing different photoactive materials, or using silicon-based photodetectors with architectures that minimize the parasitic filtering. Peterman and co-workers measured the wavelength dependence of parasitic filtering in a standard silicon-based detector. They also reported an increased bandwidth at wavelengths up to 1064 nm for an InGaAs diode as well as for a specialized, fully depleted silicon detector.[61] We have found that one commercial position sensitive detector (PSD) (Pa-
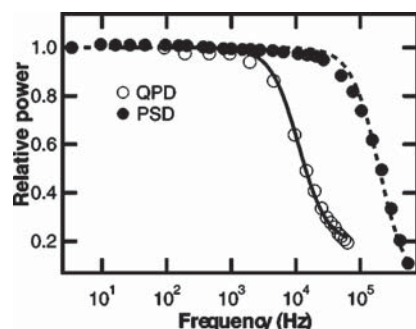
FIG. 5. Comparison of position detector frequency response at 1064 nm. Normalized frequency dependent response for a silicon quadrant photodiode (QPD) (QP50–6SD, Pacific Silicon Sensor) (open circles), and a position sensitive detector (PSD), (DL100–7PCBA, Pacific Silicon Sensor) (solid circles). 1064 nm laser light was modulated with an acousto-optic modulator and the detector output was recorded with a digital sampling scope. The response of the QPD was fit with the function: $\gamma^2+(1-\gamma^2)[1+(f/f_0)^2]^{-1}$, which describes the effects of diffusion of electron-hole pairs created outside the depletion layer (Ref. 134), where γ is the fraction of light absorbed in the diode depletion layer and f_0 is the characteristic frequency associated with light absorbed beyond the depletion layer. The fit returned an f_0 value of 11.1 kHz and a γ parameter of 0.44, which give an effective f_{3dB} of 14.1 kHz, similar to values found in Ref. 134 for silicon detectors. The QPD response was not well fit by a single pole filter response curve. The PSD response, in contrast, was fit by a single pole filter function, returning a rolloff frequency of 196 kHz. Extended frequency response at 1064 nm has also been reported for InGaAs and fully depleted silicon photodiodes (Ref. 61).

cific Silicon Detectors, which supplies output signals similar to those from a QPD, although operating on a different principle), does not suffer from parasitic filtering below ~150 kHz with 1064 nm illumination (Fig. 5).

F. Dynamic position control

Precise, calibrated lateral motion of the optical trap in the specimen plane allows objects to be manipulated and moved relative to the surface of the trapping chamber. More significantly, dynamic computer control over the position and stiffness of the optical trap allows the force on a trapped object to be varied in real time, which has been exploited to generate both force and position clamp measurement conditions.[50,81] Additionally, if the position of the optical trap is scanned at a rate faster than the Brownian relaxation time of a trapped object, multiple traps can be created by time sharing a single laser beam.[49] We consider below the different beam-steering strategies.

1. Scanning mirrors

Traditional galvanometer scanning mirrors benefited from the incorporation of feedback to improve stability and precision. Current commercial systems operate at 1–2 kHz with step response times as short as 100 μs, and with 8 μrad repeatability. The comparatively slow temporal response limits their usefulness for fast-scanning applications, but their low insertion loss and large deflection angles make them a low-cost option for slow-scanning and feedback applications. Recent advances in feedback-stabilized piezoelectric (PZ) systems have resulted in the introduction of PZ scanning mirrors. For the time being, PZ mirrors represent only a slight improvement over galvanometers, with effective op-

eration up to 1 kHz, but just 50 mrad deflection range, and only slightly better resolution and linearity than galvanometers.

2. Acousto-optic deflectors

An acousto-optic deflector (AOD) consists of a transparent crystal inside which an optical diffraction grating is generated by the density changes associated with an acoustic traveling wave of ultrasound. The grating period is given by the wavelength of the acoustic wave in the crystal, and the first-order diffracted light is deflected through an angle that depends on the acoustic frequency through $\Delta\theta=\lambda f/\nu$, where λ is the optical wavelength, and ν and f are the velocity and frequency of the acoustic wave, respectively (ν/f is the ultrasound wavelength). The diffraction efficiency is proportional to depth of the grating, and therefore to the amplitude of the acoustic wave that produced it. AODs are thereby able to control both the trap position (through deflection) and stiffness (through light level). The maximum deflection of an AOD is linearly related to its operating frequency range, and maximum deflections of somewhat over 1° are possible at 1064 nm. AODs are fast: their response times are limited, in principle, by the ratio of the laser spot diameter to the speed of sound within the crystal (~1.5 μs/mm laser diameter for TeO$_2$ crystals, slightly less for Li$_6$NbO$_3$ crystals). In practice, however, the response time of an optical trapping instrument is often limited by other components in the system. A pair of AODs can be combined in an orthogonal configuration to provide both x and y deflections of the optical trap. Due to optical losses in the AODs (an ~80% diffraction efficiency is typical), however, this scheme results in an almost 40% power loss. In addition to mediocre transmission, the diffraction efficiency of an AOD will often vary slightly as a function of its deflection. The resulting position-dependent stiffness variation of the optical trap can either be tolerated (if within acceptable margins for error), calibrated out,[53] or minimized by the selection of a particular range of operating deflections over which the diffraction efficiency is more nearly constant. In practice, however, every AOD needs to be characterized carefully before use for deflection-dependent changes in throughput.

3. Electro-optic deflectors

An electro-optic deflector (EOD) consists of a crystal in which the refractive index can be changed through the application of an external electric field. A gradient in refractive index is established in one plane along the crystal, which deflects the input light through an angle $\theta\propto lV/w^2$, where V is the applied voltage, l is the crystal length, and w is the aperture diameter. Deflections on the order of 20 mrad can be achieved with a switching time as short as 100 ns, sufficient for some optical trapping applications. Despite low insertion loss (~1%) and straightforward alignment, EODs have not been widely employed in optical trapping systems. High cost and a limited deflection range may contribute to this.

G. Piezoelectric stage

Piezoelectric stage technology has been improved dramatically through the introduction of high-precision controllers and sensitive capacitive position sensing. Stable, linear, reproducible, ultrafine positioning in three dimensions is now readily achievable with the latest generation of PZ stages. The traditional problems of hysteresis and drift in PZ devices have been largely eliminated through the use of capacitive position sensors in a feedback loop. With the feedback enabled, an absolute positional uncertainty of 1 nm has been achieved commercially. PZ stages have had an impact on practically every aspect of optical trapping. They can provide an absolute, NIST-traceable displacement measurement, from which all other position calibrations can be derived. Furthermore, these stages permit three-dimensional control of the position of the trap relative to the trapping chamber, which has previously proved difficult or inaccurate.[39] The ability to move precisely in the axial dimension, in particular, permits characterization of the longitudinal properties of the optical trap and can be used to eliminate the creep and backlash typically associated with the mechanical (gear based) focusing mechanism of the microscope. Position and force calibration routines employing the PZ stage are faster, more reproducible, and more precise than previously attainable. Finally, a piezoelectric stage can be incorporated into a force feedback loop[86,135–137] permitting constant-force records of essentially arbitrary displacement, ultimately limited by the stage travel (~ 100 μm) rather than the working range of the position detector (~ 0.3 μm), the latter being the limiting factor in feedback based on moving the optical trap.[50,59] Stage-based force-feedback permits clamping not only the transverse force, but also the axial force, and hence the polar angle through which the force is applied. Despite these advantages, PZ stages are not without their attendant drawbacks. They are comparatively expensive: a 3D stage with capacitive feedback position sensing plus a digital controller costs roughly $25,000. Furthermore, communication with the stage controller can be slower than for other methods of dynamically controlling trap position (e.g., AODs or EODs), with a maximum rate of ~ 50 Hz.[59]

H. Environmental isolation

To achieve the greatest possible sensitivity, stability, and signal-to-noise ratio in optical trapping experiments, the environment in which the optical trapping is performed must be carefully controlled. Four environmental factors affect optical trapping measurements: temperature changes, acoustic noise, mechanical vibrations, and air convection. Thermal fluctuations can lead to slow, large-scale drifts in the optical trapping instrument. For typical optical trapping configurations, a 1 K temperature gradient easily leads to micrometers of drift over a time span of minutes. In addition, acoustic noise can shake the optics that couple the laser into the objective, the objective itself, or the detection optics that lie downstream of the objective. Mechanical vibrations typically arise from heavy building equipment, e.g., compressors or pumps operating nearby, or from passing trucks on a roadway. Air currents can induce low-frequency mechanical vi-

brations and also various optical perturbations (e.g., beam deflections from gradients in refractive index produced by density fluctuations in the convected air, or light scattering by airborne dust particles), particularly near optical planes where the laser is focused.

The amount of effort and resources dedicated to reducing ambient sources of noise should be commensurate with the desired precision in the length and time scale of the measurements. Slow thermal drift may not affect a rapid or transient measurement, but could render meaningless the measurement of a slower process. Several methods of reducing noise and drift have been employed in the current generation of optical traps.

The vast majority of optical trapping instruments have been built on top of passive air tables that offer mechanical isolation (typically, -20 dB) at frequencies above ~ 2–10 Hz. For rejection of lower frequencies, actively servoed air tables are now commercially available, although we are not yet aware of their use in this field. Acoustic noise isolation can be achieved by ensuring that all optical mounts are mechanically rigid, and placing these as close to the optical table as feasible, thereby reducing resonance and vibration. Enclosing all the free-space optics will further improve both mechanical and optical stability by reducing ambient air currents. Thermal effects and both acoustical and mechanical vibration can be reduced by isolating the optical trapping instrument from noisy power supplies and heat sources. Diode pumped solid state lasers are well suited to this approach: since the laser head is fiber coupled to the pump diodes, the power supply can be situated outside of the experimental room. A similar isolation approach can be pursued with noisy computers or power supplies, and even illumination sources, whose outputs can be brought to the instrument via an optical fiber. Further improvements in noise performance and stability may require more substantial modifications, such as acoustically isolated and temperature controlled experimental rooms situated in low-vibration areas. The current generation of optical trapping instruments in our lab[59,138] are housed in acoustically quiet cleanrooms with background noise less than the NC30 (OSHA) rating, a noise level roughly equivalent to a quiet bedroom. In addition, these rooms are temperature stabilized to better than ± 0.5 K. The stability and noise suppression afforded by this arrangement has paved the way for high-resolution recording of molecular motor movement, down to the subnanometer level.[85–87]

IV. CALIBRATION

A. Position calibration

Accurate position calibration lies at the heart of quantitative optical trapping. Precise determination of the displacement of a trapped object from its equilibrium position is required to compute the applied force ($F=-\alpha x$, where F is the force, α is the optical trap stiffness, and x is the displacement from the equilibrium trapping position), and permits direct measurement of nanometer-scale motion. Several methods of calibrating the response of a position detector have been developed. The choice of method will depend on
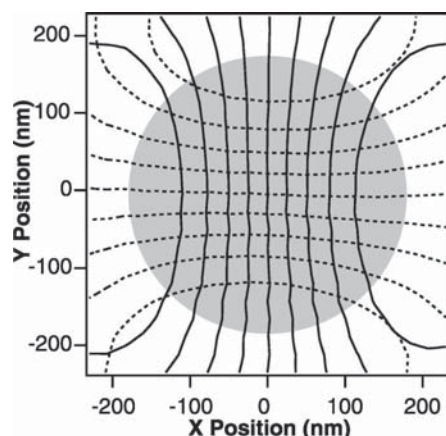
FIG. 6. Lateral two-dimensional detector calibration (adapted from Ref. 59). Contour plot of the x (solid lines) and y (dashed lines) detector response as a function of position for a 0.6 μm polystyrene bead raster scanned through the detector laser focus by deflecting the trapping laser with acousto-optic deflectors. The bead is moved in 20 nm steps with a dwell time of 50 ms per point while the position signals are recorded at 50 kHz and averaged over the dwell time at each point. The x contour lines are spaced at 2 V intervals, from 8 V (leftmost contour) to −8 V (rightmost contour). The y contour lines are spaced at 2 V intervals, from 8 V (bottom contour) to −8 V (top contour). The detector response surfaces in both the x and y dimensions are fit to fifth order two-dimensional polynomials over the shaded region, with less than 2 nm residual root mean square (rms) error. Measurements are confined to the shaded region, where the detector response is single valued.

the position detection scheme, the ability to move the trap and/or the stage, the desired accuracy, and the expected direction and magnitude of motion in the optical trap during an experiment. The most straightforward position calibration method relies on moving a bead through a known displacement across the detector region while simultaneously recording the output signal. This operation can be performed either with a stuck bead moved by a calibrated displacement of the stage, or with a trapped bead moved with a calibrated displacement of a steerable trap.

Position determination using a movable trap relies on initial calibration of the motion of the trap itself in the specimen plane against beam deflection, using AODs or deflecting mirrors. This is readily achieved by video tracking a trapped bead as the beam is moved.[49] Video tracking records can be converted to absolute distance by calibrating the charge coupled device (CCD) camera pixels with a ruled stage micrometer (10 μm divisions or finer),[49,50] or by video tracking the motion of a stuck bead with a fully calibrated piezoelectric stage.[59] Once the relationship between beam deflection and trap position is established, the detector can then be calibrated in one or both lateral dimensions by simply moving a trapped object through the detector active area and recording the position signal.[50,59,81] Adequate two-dimensional calibration may often be obtained by moving the bead along two orthogonal axes in an "X" pattern. However, a more complete calibration requires raster scanning the trapped bead to cover the entire active region of the sensor.[59] Figure 6 displays the two-dimensional detector calibration for a 0.6 μm bead, raster scanned over the detector region using an AOD-driven optical trap. A movable optical trap is typically used with either an imaging position detector, or a second low-power laser for laser-based detection (described above). Cali-

brating by moving the trap, however, offers several advantages. Position calibration can be performed individually for each object trapped, which eliminates errors arising from differences among nominally identical particles, such as uniform polystyrene beads, which may exhibit up to a 5% coefficient of variation in diameter. Furthermore, nonspherical or nonidentical objects, such as bacteria or irregularly shaped particles, can be calibrated on an individual basis prior to (or after) an experimental measurement. Because the object is trapped when it is calibrated, the calibration and detection necessarily take place in the same axial plane, which precludes calibration errors arising from the slight axial dependence of the lateral position signals.

Laser-based detection used in conjunction with a movable trap affords additional advantages. Because the trapping and detection lasers are separate, the focal position of the two can be moved relative to one another in the axial dimension. The maximum lateral sensitivity and minimum variation of lateral sensitivity with axial position occur at the focus of the detection laser. The axial equilibrium position of a trapped object, however, lies above the focus due to the scattering force. Since the detection and trapping lasers are uncoupled, the focus of the detection laser can be made coincident with the axial position of the trapped object, thereby maximizing the detector sensitivity while minimizing the axial dependence of the lateral sensitivity.[59] An additional benefit to using an independent detection laser is that it can be more weakly focused to a larger spot size, since it does not need to trap, thereby increasing the usable detection range. Beyond the added complication and cost of building a movable trap, calibrating with a movable trap has some important limitations. The calibration is limited to the two lateral dimensions, which may be inadequate for experiments where the trapped bead is displaced significantly in the axial dimension.[39,82] Due to the ~4–6-fold lower trap stiffness in the axial dimension, a primarily lateral force pulling an object out of the trapping zone may result in a significant axial displacement. In practice, this situation arises when the trapped object is tethered to the surface of the trapping chamber, e.g., when a bead is attached by a strand of DNA bound at its distal end to the coverglass.[39,82,88,135–137] Accurate determinations of displacement and trapping force in such experiments require axial, as well as lateral, position calibration.

Position calibration is most commonly accomplished by moving a bead fixed to the surface through the detection region and recording the detector output as a function of position. Traditionally, such calibrations were performed in one or two lateral dimensions. The advent of servo-stabilized, 3D piezoelectric (pz) stages has made such calibrations more accurate, easier to perform and—in conjunction with an improved theoretical understanding of the axial position signal—has permitted a full 3D position calibration of an optical trap.[62–64] Whereas full 3D calibration is useful for tracking the complete motion of an object, it is cumbersome and unnecessary when applying forces within a plane defined by one lateral direction and the optical axis. When the trapped object is tethered to the surface of the trapping chamber, for example, it is sufficient to calibrate the axial
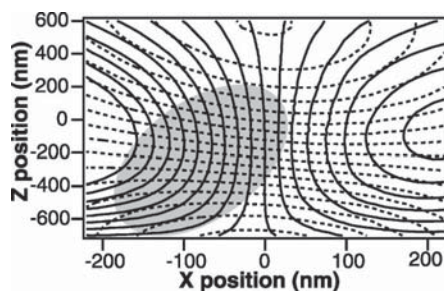
FIG. 7. Axial two-dimensional detector calibration. Contour plot of the lateral (solid lines) and axial (dashed lines) detector response as a function of x (lateral displacement) and z (axial displacement) of a stuck 0.5 μm polystyrene bead moving through the laser focus. A stuck bead was raster scanned in 20 nm steps in x and z. The detector signals were recorded at 4 kHz and averaged over 100 ms at each point. The lateral contour lines are spaced at 1 V intervals, from −9 V (leftmost contour) to 7 V (rightmost contour). The axial contour lines are spaced at 0.02 intervals (normalized units). Measurements are confined to the region of the calibration shaded in gray, over which the surfaces of x and z positions as a function of lateral and axial detector signals were fit to seventh order two-dimensional polynomial functions with less than 5 nm residual rms error.

and the single lateral dimension in which the force is applied. Figure 7 displays the results of such a two-dimensional ("x–z") position calibration for a 0.5 μm bead stuck to the surface of the trapping chamber. The bead was stepped through a raster scan pattern in x (lateral dimension) and z (axial dimension) while the position signals were recorded. Using a stuck bead to calibrate the position detector has some limitations and potential pitfalls. Because it is difficult, in general, to completely immobilize an initially trapped particle on the surface, it is not feasible to calibrate every particle. Instead, an average calibration derived from an ensemble of stuck beads must be measured. Furthermore, the stuck-bead calibration technique precludes calibrating nonspherical or heterogeneous objects, unless these can be attached to the surface (and stereospecifically so) prior to, or after, the experimental measurements. Due to the axial dependence of the lateral position signals ("x–z crosstalk"), using a stuck bead to calibrate only the lateral dimension is prone to systematic error. Without axial position information, it is difficult to precisely match the axial position of a stuck bead with the axial position of a trapped bead. Optically focusing on a bead cannot be accomplished with an accuracy better than ~100 nm, which introduces uncertainty and error in lateral position calibrations for which the axial position is set by focusing. Therefore, even when only the lateral dimensions are being calibrated, it is useful to measure the axial position signal to ensure that the calibration is carried out in the appropriate axial plane.

1. Absolute axial position and measurement of the focal shift

The absolute axial position of a trapped object above the surface of the trapping chamber is an important experimental parameter, because the hydrodynamic drag on an object varies nonlinearly with its height above the surface, due to proximal wall effects (see below and Ref. 9). Absolute axial position measurements may be especially important in situations where the system under investigation is attached to the
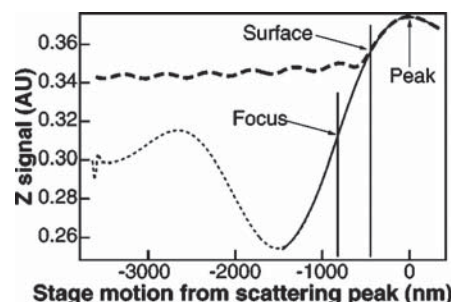

FIG. 8. Axial position signals for a free (heavy dashed line) and stuck (light dashed line) bead as the stage was scanned in the axial direction. All stage motion is relative to the scattering peak, which is indicated on the right of the figure. The positions of the surface (measured) and the focus [calculated from Eq. (5)] are indicated by vertical lines. The axial detection fit [Eq. (5)] to the stuck bead trace is shown in the region around the focus as a heavy solid line.

surface and to a trapped object, as is often the case in biological applications. Force–extension relationships, for example, depend on the end-to-end extension of the molecule, which can only be determined accurately when the axial position of the trapped object with respect to the surface is known. Axial positioning of a trapped object depends on finding the location of the surface of the chamber and moving the object relative to this surface by a known amount. The problem is complicated by the focal shift that arises when focusing through a planar interface between two mismatched indices of refraction e.g., between the coverglass ($n_{glass} \sim 1.5$) and the aqueous medium ($n_{water} \sim 1.3$).[139–144] This shift introduces a fixed scaling factor between a vertical motion of the chamber surface and the axial position of the optical trap within the trapping chamber. The focal shift is easily computed from Snell's law for the case of paraxial rays, but it is neither straightforward to compute nor to measure experimentally when high NA objectives are involved.[144] Absolute axial position determination has previously been assessed using fluorescence induced by an evanescent wave,[131] by the analysis of interference or diffraction patterns captured with video,[113,145] or through the change in hydrodynamic drag on a trapped particle as it approaches the surface.[39] These techniques suffer from the limited range of detectable motion for fluorescence-based methods, and by the slow temporal response of video and drag-force-based measurements.

The position detector sum signal (QPD or PSD output), which is proportional to the total incident intensity at the back focal plane of the condenser, provides a convenient means of both accurately locating the surface of the trapping chamber and measuring the focal shift. In conjunction, these measurements permit absolute positioning of a trapped object with respect to the trapping chamber surface. The detector sum signal as a function of axial stage position for both a stuck bead and a trapped bead are shown in Fig. 8. The stuck bead trace represents the axial position signal of a bead moving relative to the trap. As the bead moves through the focus of the laser (marked on the figure), the phase of light scattered from the bead changes by 180° relative to the unscattered light, modulating the intensity distribution at the back focal plane of the condenser. The region between the extrema

of the stuck-bead curve is well described by the expression for axial sensitivity derived by Pralle and co-workers:[62]

$$\frac{I_z}{I}(z) \propto \left(1 + \left(\frac{z}{z_0}\right)^2\right)^{1/2} \sin[\tan^{-1}(z/z_0)], \qquad (5)$$

where an overall scaling factor has been ignored, z is the axial displacement from the beam waist, and $z_0 = \pi w_0^2/\lambda$ is the Raleigh length of the focus, with beam waist w_0 at wavelength λ. The phase difference in the scattered light is described by the arctangent term, while the prefactor describes the axial position dependent intensity of the scattered light. The fit returns a value for the beam waist, $w_0 = 0.436 \ \mu$m. The equilibrium axial position of a trapped bead corresponds to a displacement of 0.379 μm from the laser focus. A stuck bead scan can also be useful for determining when a free bead is forced onto the surface of the cover slip.

As a trapped bead is forced into contact with the surface of the chamber by the upward stage motion, the free and stuck bead signals merge and eventually become indistinguishable (Fig. 8). The approximate location of the surface with respect to the position of a trapped bead can be determined by finding the point at which both curves coincide. Brownian motion of the trapped bead, however, will shift this point slightly, in a stiffness-dependent manner that will introduce a small uncertainty in the measured position of the surface. The scattering peak in Fig. 8, however, serves as an easily identifiable fiducial reference from which the trapped bead can be moved an absolute distance by subsequent stage motion. In this manner, trapped particles can be reproducibly positioned at a fixed (but uncertain) distance relative to the surface. In order to obtain a precise location of the trapped particle above the surface, both the position of the scattering peak with respect to the surface and the focal shift must be determined. This may be accomplished, for example, by a one-time measurement of the drag on a trapped bead at a series of positions above the scattering peak. The interaction of a sphere with the boundary layer of water near a surface leads to an increase in the hydrodynamic drag β, which can be estimated by Faxen's law for the approximate drag on a sphere:[9]

$$\beta = \frac{6\pi\eta a}{1 - \frac{9}{16}\left(\frac{a}{h}\right) + \frac{1}{8}\left(\frac{a}{h}\right)^3 - \frac{45}{256}\left(\frac{a}{h}\right)^4 - \frac{1}{16}\left(\frac{a}{h}\right)^5}, \qquad (6)$$

which depends only on the bead radius a, the distance above the surface h, and the viscosity of the liquid η. By measuring the rolloff frequency or the displacement of the trapped bead as the stage is oscillated (see below), the drag force can be determined at different axial stage positions relative to the scattering peak and normalized to the calculated asymptotic value, the Stokes drag coefficient, $6\pi\eta a$. The resulting curve (Fig. 9) is described by a two parameter fit to Eq. (6): a scaling parameter that represents the fractional focal shift and an offset parameter related to the distance between the scattering peak and the coverglass surface. The fit parameters from the curve in Fig. 9 allow absolute positioning of a trapped particle with respect to the surface. The uncertainty in the axial position amounts to roughly 3% of the bead-surface separation, with the residual uncertainty largely due
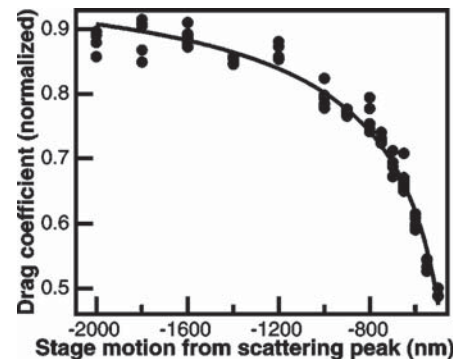

FIG. 9. Normalized drag coefficient (β_0/β, where β_0 is the Stokes drag on the sphere: $6\pi\eta a$) as a function of distance from the scattering peak. The normalized inverse drag coefficient (solid circles) was determined through rolloff measurements and from the displacement of a trapped bead as the stage was oscillated. The normalized inverse drag coefficient was fit to Faxen's law [Eq. (6)] with a height offset ε and scaling parameter δ, which is the fractional focal shift, as the only free parameters: $\beta_0/\beta = 1 - (9/16) \times [a\delta^{-1}(z-\varepsilon)^{-1}] + \frac{1}{8}[a\delta^{-1}(z-\varepsilon)^{-1}]^3 - (45/256)[a\delta^{-1}(z-\varepsilon)^{-1}]^4 - (1/16)[a\delta^{-1}(z-\varepsilon)^{-1}]^5$, where a is the bead radius, z is the motion of the stage relative to the scattering peak, β_0 is the Stoke's drag on the bead, ($6\pi\eta a$), and β is the measured drag coefficient. The fit returned a fractional focal shift δ of 0.82 ± 0.02 and an offset ε of 161 nm. The position of the surface relative to the scattering peak is obtained by setting the position of the bead center, $\delta(z-\varepsilon)$ equal to the bead radius a, which returns a stage position of 466 nm above the scattering peak, as indicated in Fig. 8.

to the estimate of the focal shift (which leads to a relative rather than an absolute uncertainty). The position of the surface, calculated from the fit parameters of Fig. 9, is indicated in Fig. 8. The focal shift was 0.82 ± 0.02, i.e., the vertical location of the laser focus changed by 82% of the vertical stage motion.

The periodic modulation of the axial position signal as a trapped bead is displaced from the surface (Fig. 8) can be understood in terms of an étalon picture.[146] Backscattered light from the trapped bead reflects from the surface and interferes with forward-scattered and unscattered light in the back focal plane of the condenser. The phase difference between these two fields includes a constant term that arises because of the Gouy phase and another term that depends on the separation between the bead and the surface. The spatial frequency of the intensity modulation is given by $d = \lambda/(2n_m)$, where d is the separation between the bead and the cover slip, λ is the vacuum wavelength of the laser, and n_m is the index of refraction of the medium. This interference signal supplies a second and much more sensitive means to determine the focal shift. The motion of the stage (d_s) and motion of the focus (d_f) are related through a scaling parameter f_s equal to the focal shift $d_f = f_s d_s$. The interference signal is observed experimentally by stage translations. The measured spatial frequency will be given by $d_s = \lambda/(2n_m f_s)$, which can be rearranged to solve for the focal shift $f_s = \lambda/(2n_m d_s)$. The focal shift determined in this manner was 0.799 ± 0.002, which is within the uncertainty of the focal shift determined by hydrodynamic drag measurements (Fig. 9). The true focal shift with a high NA lens is more pronounced than the focal shift computed in the simple paraxial limit, given (from Snell's law) by the ratio of the indices of refraction: $n_m/n_{imm} = 0.878$ for the experimental conditions,

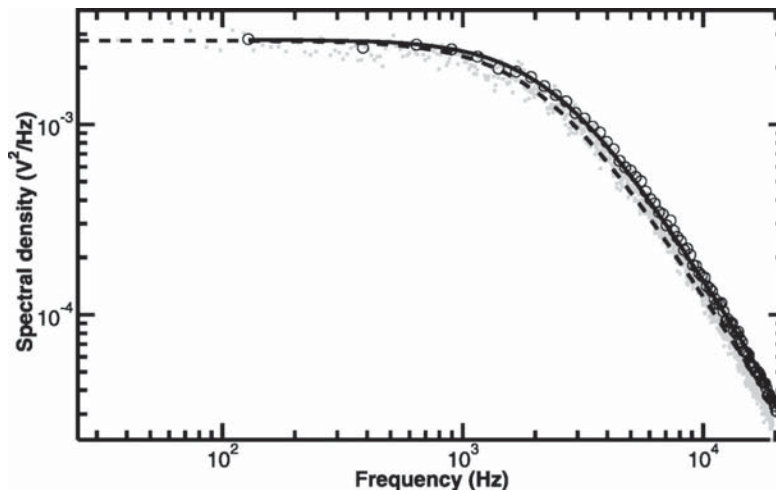FIG. 10. Power spectrum of a trapped bead. Power spectrum of a 0.5 μm polystyrene bead trapped 1.2 μm above the surface of the trapping chamber recorded with a PSD (gray dots). The raw power spectrum was averaged over 256 Hz windows on the frequency axis (black circles) and fit (black line) to a Lorentzian [Eq. (7)] corrected for the effects of the antialiasing filter, frequency dependent hydrodynamic effects, and finite sampling frequency, as described by Berg–Sørensen and Flyvbjerg (Ref. 148). The rolloff frequency is 2.43 kHz, corresponding to a stiffness of 0.08 pN/nm. For comparison the raw power spectrum was fit to an uncorrected Lorentzian (dashed line), which returns a rolloff frequency of 2.17 kHz. Whereas the discrepancies are on the order 10% for a relatively weak trap, they generally become more important at higher rolloff frequencies.

where n_m is the index of the aqueous medium (1.33) and n_{imm} is the index of the objective immersion oil (1.515). The discrepancy should not be surprising, because the paraxial ray approximation does not hold for the objectives used for optical trapping.[146] The interference method employed to measure the focal shift is both easier and more accurate than the drag-force method presented earlier.

2. Position calibration based on thermal motion

A simple method of calibrating the position detector relies on the thermal motion of a bead of known size in the optical trap.[122] The one-sided power spectrum for a trapped bead is[9]

$$S_{xx}(f) = \frac{k_B T}{\pi^2 \beta (f_0^2 + f^2)},\qquad(7)$$

where $S_{xx}(f)$ is in units of displacement^2/Hz, k_B is Boltzmann's constant, T the absolute temperature, β is the hydrodynamic drag coefficient of the object (e.g., $\beta = 6\pi\eta a$ for Stokes drag on a sphere of radius a in a medium with viscosity η), and f_0 is the rolloff frequency, related to the trap stiffness through $f_0 = \alpha(2\pi\beta)^{-1}$ for a stiffness α (see below). The detector, however, measures the uncalibrated power spectrum $S_{vv}(f)$, which is related to the true power spectrum by $S_{vv}(f) = \rho^2 \cdot S_{xx}(f)$, where ρ represents the linear sensitivity of the detector (in volts/unit distance). The sensitivity can be found by considering the product of the power spectrum and the frequency squared $S_{xx}(f) \cdot f^2$, which asymptotically approaches the limit $k_B T(\pi^2\beta)^{-1}$ for $f \gg f_0$. Inserting the relationship between the displacement power spectrum and the uncalibrated detector spectrum in this expression and rearranging gives

$$\rho = [S_{vv}(f)\pi^2\beta/k_B T]^{1/2}.\qquad(8)$$

This calibration method has been shown to agree to within $\sim$20% of the sensitivity measured by more direct means, such as those discussed above.[122] An advantage to the

method is that it does not require any means of precisely moving a bead to calibrate the optical trap. However, the calibration obtained by this method is valid only for small displacements, for which a linear approximation to the position signal is valid. In addition, the system detection bandwidth must be adequate to record accurately the complete power spectrum without distortion, particularly in the high frequency regime. System bandwidth considerations are treated more fully in conjunction with stiffness determination, discussed below.

B. Force calibration–stiffness determination

Forces in optical traps are rarely measured directly. Instead, the stiffness of the trap is first determined, then used in conjunction with the measured displacement from the equilibrium trap position to supply the force on an object through Hooke's law: $F = -\alpha x$, where F is the applied force, α is the stiffness, and x is the displacement. Force calibration is thus reduced to calibrating the trap stiffness and separately measuring the relative displacement of a trapped object. A number of different methods of measuring trap stiffness, each with its attendant strengths and drawbacks, have been implemented. We discuss several of these.

1. Power spectrum

When beads of known radius are trapped, the physics of Brownian motion in a harmonic potential can be exploited to find the stiffness of the optical trap. The one-sided power spectrum for the thermal fluctuations of a trapped object is given by Eq. (7), which describes a Lorentzian. This power spectrum can be fit with an overall scaling factor and a rolloff frequency, $f_0 = \alpha(2\pi\beta)^{-1}$ from which the trap stiffness (α) can be calculated if the drag (β) on the particle is known (Fig. 10). For a free sphere of radius a in solution far from any surfaces, the drag is given by the usual Stokes relation $\beta = 6\pi\eta a$, where η is the viscosity of the medium. For a bead

trapped nearer the surface of the trapping chamber, additional drag arises from wall effects and must be considered: Faxen's law [Eq. (6)] is appropriate for estimating the drag due to lateral motion. Axial stiffness is also measured via the power spectrum of the axial position signal, but the corrections to the axial drag due to wall effects are larger than those for the lateral drag. The drag on a sphere moving normal to a surface is[147]

$$\beta = \beta_0 \frac{4}{3} \sinh \alpha \sum_{n=1}^{\infty} \frac{n(n+1)}{(2n-1)(2n+3)}$$
$$\times \left[\frac{2 \sinh(2n+1)\alpha + (2n+1)\sinh 2\alpha}{4\sinh^2\left(n+\frac{1}{2}\right)\alpha - (2n+1)^2\sinh^2\alpha} - 1 \right], \qquad (9)$$

where

$$\alpha = \cosh^{-1}\left(\frac{h}{a}\right) = \ln\left\{\frac{h}{a} + \left[\left(\frac{h}{a}\right)^2 - 1\right]^{1/2}\right\},$$

h is the height of the center of the sphere above the surface, and $\beta_0 = 6\pi\eta a$ is the Stokes drag. The sum converges fairly quickly and ~ 10 terms are required to achieve accurate results. Whereas it is tempting to measure trap stiffness well away from surfaces to minimize hydrodynamic effects, spherical aberrations in the focused light will tend to degrade the optical trap deeper in solution, particularly in the axial dimension. Spherical aberrations lead to both a reduction in peak intensity and a smearing-out of the focal light distribution in the axial dimension.

Determining the stiffness of the optical trap by the power spectrum method requires a detector system with sufficient bandwidth to record faithfully the power spectrum well beyond the rolloff frequency (typically, by more than 1 order of magnitude). Lowpass filtering of the detector output signal, even at frequencies beyond the apparent rolloff leads directly to a numerical underestimate of the rolloff frequency and thereby to the stiffness of the optical trap. Errors introduced by low pass filtering become more severe as the rolloff frequency of the trap approaches the rolloff frequency of the electrical filter. Since the trap stiffness is determined solely from the rolloff of the Lorentzian power spectrum, this method is independent of the position calibration, per se. In addition to determining the stiffness, the power spectrum of a trapped bead serves as a powerful diagnostic tool for optical trapping instruments: alignment errors of either the optical trap or the position detection system lead to non-Lorentzian power spectra, which are easily scored, and extraneous sources of instrument noise can generate additional peaks in the power spectrum.

The measurement and accurate fitting of power spectra to characterize trap stiffness was recently investigated by Berg-Sørensen and Flyvbjerg,[148,149] who developed an improved expression for the power spectrum that incorporates several previously ignored corrections, including the frequency dependence of the drag on the sphere, based on an extension of Faxen's law for an oscillating sphere [Faxen's law, Eq. (6), only holds strictly in the limit of *constant* velocity]. These extra terms encapsulate the relevant physics for a sphere moving in a harmonic potential with viscous damping. In addition to this correction, the effects of finite sampling frequency and signal filtering during data acquisition (due to electronic filters or parasitic filtering by the photosensor) were included in fitting the experimental power spectrum. The resulting fits determine the trap stiffness with an uncertainty of $\sim 1\%$ and accurately describe the shape of the measured spectra. This work underscores the importance of characterizing and correcting the frequency response of the position detection system to obtain accurate stiffness measurements. Figure 10 illustrates a comparison between the fit obtained with the improved fitting routine and an uncorrected fit.

The power spectrum of a trapped bead can also be used to monitor the sample heating due to partial absorption of the trapping laser light. Heating of the trapping medium explicitly changes the thermal kinetic energy term ($k_B T$) in the power spectrum [Eq. (7)] and implicitly changes the drag term as well, $\beta = 6\pi\eta(T)a$, through its dependence on viscosity, which is highly temperature dependent. Peterman and co-workers were able to assess the temperature increase as a function of trapping laser power by determining the dependence of the Lorentzian fit parameters on laser power.[100]

2. Equipartition

The thermal fluctuations of a trapped object can also be used to obtain the trap stiffness through the Equipartition theorem. For an object in a harmonic potential with stiffness α:

$$\tfrac{1}{2} k_B T = \tfrac{1}{2} \alpha \langle x^2 \rangle, \qquad (10)$$

where k_B is Boltzmann's constant, T is absolute temperature, and x is the displacement of the particle from its trapped equilibrium position. Thus, by measuring the positional variance of a trapped object, the stiffness can be determined. The variance $\langle x^2 \rangle$ is intimately connected to the power spectrum, of course: it equals the integral of the position power spectrum, i.e., the spectrum recorded by a calibrated detector. Besides its simplicity, a primary advantage of the Equipartition method is that it does not depend explicitly on the viscous drag of the trapped particle. Thus, the shape of the particle, its height above the surface, and the viscosity of the medium need not be known to measure the trap stiffness (although, in fairness, both the particle shape and the optical properties of the medium will influence the position calibration itself). The bandwidth requirements of the position detection system are the same as for the power spectral approach, with the additional requirement that the detector must be calibrated. Unlike the power spectral method however, the variance method does not provide additional information about the optical trap or the detection system. For this reason, care should be taken when measuring the stiffness with the Equipartition method. Because variance is an intrinsically *biased estimator* (it is derived from the square of a quantity, and is therefore always positive), any added noise and drift in position measurements serve only to increase the overall variance, thereby decreasing the apparent stiffness estimate. In contrast, low pass filtering of the position signal results in a lower variance and an apparent increase in stiffness.

3. Optical potential analysis

A straightforward extension of the Equipartition method involves determining the complete distribution of particle positions visited due to thermal motions, rather than simply the variance of that distribution. The probability for the displacement of a trapped object in a potential well will be given by a Boltzmann distribution

$$P(x) \propto \exp\left(\frac{-U(x)}{k_B T}\right) = \exp\left(\frac{-\alpha x^2}{2 k_B T}\right), \tag{11}$$

where $U(x)$ is the potential energy and $k_B T$ is the thermal energy. When the potential is harmonic, this distribution is a simple Gaussian parametrized by the trap stiffness α. When the potential is anharmonic, the position histogram can be used, in principle, to characterize the shape of the trapping potential by taking the logarithm and solving for $U(x)$. In practice, this approach is not especially useful without a considerable body of low-noise/low-drift position data, since the wings of the position histogram—which carry the most revealing information about the potential—hold the fewest counts and therefore have the highest relative uncertainty.

4. Drag force method

The most direct method of determining trap stiffness is to measure the displacement of a trapped bead from its equilibrium position in response to viscous forces produced by the medium, generated by moving the stage in a regular triangle wave or sinusoidal pattern. Since forces arise from the hydrodynamics of the trapped object, the drag coefficient, including any surface proximity corrections, must be known. For the case of a sinusoidal driving force of amplitude A_0 and frequency f, the motion of the bead is

$$x(t) = \frac{A_0 f}{\sqrt{f_0^2 + f^2}} \exp[-i(2\pi f t - \varphi)],$$

$$\varphi = -\tan^{-1}(f_0/f), \tag{12}$$

where f_0 is the characteristic rolloff frequency (above), and φ is the phase delay. Both the amplitude and the phase of the bead motion can be used to provide a measure of trap stiffness.

A triangular driving force of amplitude A_0 and frequency f results in a square wave of force being applied to the bead. For each period of the motion the bead trajectory is

$$x(t) = \frac{\beta A_0 f}{2\alpha}\left[1 - \exp\left(-\frac{\alpha}{\beta}t\right)\right], \tag{13}$$

where α is the trap stiffness and β is the drag coefficient of the bead, including Faxen's law corrections. Due to the finite response time of the stage, the exponential damping term is convolved with the response time of the stage. Therefore, only the asymptotic value $(\beta A_0 f / 2\alpha)$ should be used to obtain a reliable estimate of trap stiffness. Drag-force measurements are slow compared with the thermal motion of the particle, so the bandwidth requirements of the detection system are significantly relaxed. Increasing the amplitude or the frequency of the stage motion generates larger displacements of the trapped bead. By measuring the stiffness as a function of bead displacement, the linear region of the trap over
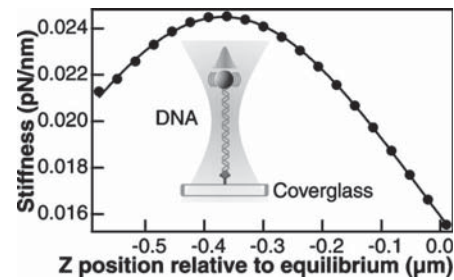

FIG. 11. Axial dependence of lateral stiffness. The experimental geometry for these measurements is depicted in the inset. A polystyrene bead is tethered to the surface of the cover glass through a long DNA tether. The stage was moved in the negative z direction (axial), which pulls the bead towards the laser focus, and the lateral stiffness was determined by measuring the lateral variance of the bead. The data (solid circles) are fit with the expression for a simple dipole [Eq. (14)], with the power in the specimen plane, the beam waist, and an axial offset as free parameters.

which the stiffness is constant can be easily determined.

A variation on the drag force method of stiffness calibration, sometimes called step response calibration, involves rapidly displacing the trap by a small, fixed offset and recording the subsequent trajectory of the bead. The bead will return to its equilibrium position in an exponentially damped manner, with a time constant of α/β as in Eq. (13).

5. Direct measurement of optical force

The lateral trapping force arises from the momentum transfer from the incident laser light to the trapped object, which leads to a change in the direction of the scattered light (Fig. 1). Measuring the deflection of the scattered laser beam with a QPD or other position sensitive detector therefore permits direct measurement of the momentum transfer, and hence the force, applied to the trapped object—assuming that all the scattered light can be collected.[38,57,104] An expression relating the applied force to the beam deflection was presented by Smith et al.:[38] $F = I/c \cdot (NA) \cdot X/R_{ba}$ where F is the force, I is the intensity of the laser beam, c is the speed of light, NA is the numerical aperture, X is the deflection of the light, and R_{ba} is the radius of the back aperture of the microscope objective. In principle, this approach is applicable to any optical trapping configuration. However, because it necessitates measuring the total intensity of scattered light, it has only been implemented for relatively low NA, counter-propagating optical traps, where the microscope objective entrance pupils are underfilled. In single-beam optical traps, it is impractical to collect the entirety of the scattered light, owing to the higher objective NA combined with an optical design that overfills the objective entrance pupil.

6. Axial dependence of lateral stiffness

Three-dimensional position detection facilitates measurement of the axial stiffness and mapping of the lateral stiffness as a function of axial position in the trap. Due to the high refractive index of polystyrene beads typically used in optical trapping studies, there is a correspondingly large scattering force in the axial direction. Consequently, the axial equilibrium position of a trapped polystyrene bead tends to lie well beyond the focus, where the lateral intensity gradient—and hence the lateral stiffness—are significantly
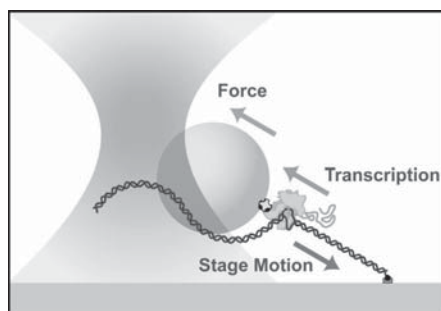
FIG. 12. Cartoon of the experimental geometry (not to scale) for single-molecule transcription experiment. Transcribing RNA polymerase with nascent RNA (gray strand) is attached to a polystyrene bead. The upstream end of the duplex DNA (black strands) is attached to the surface of a flowchamber mounted on a piezoelectric stage. The bead is held in the optical trap at a predetermined position from the trap center, which results in a restoring force exerted on the bead. During transcription, the position of the bead in the optical trap and hence the applied force is maintained by moving the stage both horizontally and vertically to compensate for motion of the polymerase molecule along the DNA (adapted from Ref. 87).
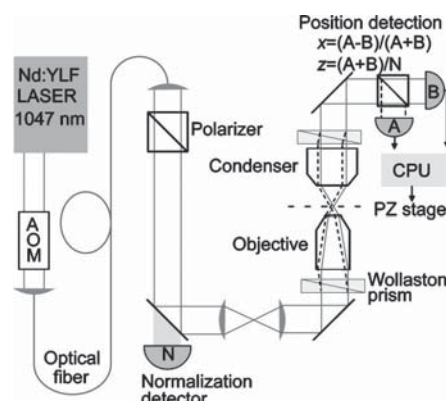

FIG. 13. The optical trapping interferometer. Light from a Nd:YLF laser passes through an acoustic optical modulator (AOM), used to adjust the intensity, and is then coupled into a single-mode polarization-maintaining optical fiber. Output from the fiber passes through a polarizer to ensure a single polarization, through a 1:1 telescope and into the microscope where it passes through the Wollaston prism and is focused in the specimen plane. The scattered and unscattered light is collected by the condenser, is recombined in the second Wollaston prism, then the two polarizations are split in a polarizing beamsplitter and detected by photodiodes A and B. The bleedthrough on a turning mirror is measured by a photodiode (N) to record the instantaneous intensity of the laser. The signals from the detector photodiodes and the normalization diode are digitized and saved to disk. The normalized difference between the two detectors (A and B) gives the lateral, x displacement, while the sum signal (A+B) normalized by the total intensity (N) gives the axial, z displacement.

reduced from their values at the focus. In experiments in which beads are displaced from the axial equilibrium position, the change in lateral trapping strength can be significant. The variation of lateral stiffness as a function of axial position was explored using beads tethered by DNA (1.6 μm) to the surface of the flow chamber (Fig. 11, inset). Tethered beads were trapped and the attachment point of the tether was determined and centered on the optical axis.[39] The bead was then pulled vertically through the trap, i.e., along the axial dimension, by lowering the stage in 20 nm increments. At each position, the lateral stiffness of the trap was ascertained by recording its variance, using the Equipartition method. The axial force applied to the bead tether can increase the apparent lateral stiffness, and this effect can be computed by treating the tethered bead as a simple inverted pendulum.[150,151] In practice, the measured increase in lateral stiffness (given by $\alpha_x = F_a/l$, where α_x is the lateral stiffness, F_a is the axial force on the bead, and l is the length of the tether) resulted in less than a 3% correction to the stiffness and was thereafter ignored in the analysis. An average of 12 measurements is shown in Fig. 11, along with a fit to the lateral stiffness based on a simple dipole and zero-order Gaussian beam model.[152]

$$\alpha_x(z) = \frac{8 n_m p}{c w_0} \left(\frac{a}{w_0} \right)^3 \left(\frac{m^2 - 1}{m^2 + 2} \right) \left(1 + \left(\frac{z}{z_0} \right)^2 \right)^{-2}, \quad (14)$$

where n_m is the index of refraction of the medium, p is the laser power in the specimen plane, c is the speed of light, m is the ratio of the indices of refraction of the bead and the medium, and w_0, z and z_0 are the beam diameter at the waist, the axial displacement of the particle relative to the focus, and the Raleigh range, respectively (as previously defined). The data are well fit by this model with the exception of the laser power, which was sixfold lower than the actual power estimated in the specimen plane. A significant discrepancy was anticipated since it had been previously shown that for particle sizes on the order of the beam waist, the dipole approximation greatly overestimates the trap stiffness.[152] The other two parameters of interest are the beam waist and the

equilibrium axial position of the bead in the trap. The fit returned distances of 0.433 μm for the beam waist and 0.368 μm for the offset of the bead center from the focal point. These values compare well with the values determined from the fit to the axial position signal, which were 0.436 and 0.379 μm, respectively (see above). The variation in lateral stiffness between the optical equilibrium position and the laser focus was substantial: a factor of l.5 for the configuration studied.

V. TRANSCRIPTION STUDIED WITH A TWO-DIMENSIONAL STAGE-BASED FORCE CLAMP

Our interest in extending position detection techniques to include the measurement of force and displacement in the axial dimension arose from the study of processive nucleic acid enzymes moving along DNA (Fig. 12). The experimental geometry, in which the enzyme moving along the DNA pulls on a trapped bead, results in motion of the bead in a plane defined by the direction of the lateral force and the axial dimension. In previous experiments, the effects of axial motion had been calculated and estimated, but not directly measured or otherwise calibrated.[39,82] Improvements afforded by three-dimensional piezoelectric stages permitted the direct measurement of, and control over, the separate axial and lateral motions of the trapped bead. We briefly describe this instrument and the implementation of a two-dimensional force clamp to measure transcription by a single molecule of RNA polymerase.[87]

The optical layout and detection scheme are illustrated in Fig. 13. An existing optical trap[39,153] was modified by adding a normalizing photodetector to monitor the bleedthrough of the trapping laser after a 45° dielectric mirror and a
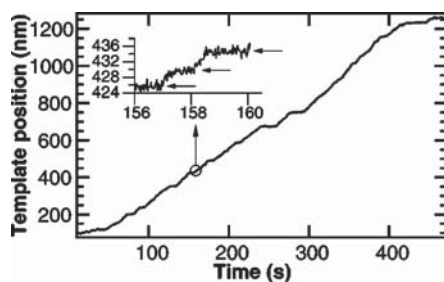
FIG. 14. Two-dimensional, stage based force clamp. Position record of a single RNA polymerase molecule transcribing a 3.5 kbp (1183 nm) DNA template under 18 pN of load. The x and z position signals were low pass filtered at 1 kHz, digitized at 2 kHz, and boxcar averaged over 40 points to generate the 50 Hz feedback signals that controlled the motion of the piezo-electric stage. Motion of the stage was corrected for the elastic compliance of the DNA (Ref. 39) to recover the time-dependent contour length, which reflects the position of the RNA polymerase on the template. Periods of roughly constant velocity are interrupted by pauses on multiple timescales. Distinct pauses can be seen in the trace, while shorter pauses (~1 s) can be discerned in the expanded region of the trace (inset: arrows).

feedback-stabilized three-axis piezoelectric stage (Physik Instrumente P-517.3CD and E710.3CD digital controller) to which the trapping chamber was affixed. The optical trap was built around an inverted microscope (Axiovert 35, Carl Zeiss) equipped with a polarized Nd:YLF laser (TFR, Spectra Physics, $\lambda = 1047$ nm, TEM_{00}, 2.5 W) that is focused to a diffraction-limited spot through an objective (Plan Neofluar $100\times$, 1.3 NA oil immersion). Lateral position detection based on polarization interferometry was implemented. The trapping laser passes through a Wollaston prism below the objective producing two orthogonally polarized and slightly spatially separated spots in the specimen plane; these act as a single trap. The light is recombined by a second Wollaston prism in the condenser, after which it passes through a quarter-wave plate and a polarizing beamsplitter. Two photodetectors measure the power in each polarization, and the difference between them, normalized by their sum, supplies the lateral position signal. The sum of the detector signals normalized by the incident laser power (from the normalizing detector) provides the axial position signal.[62,64] The axial position signal is a small fraction of the total intensity and is roughly comparable to the intensity noise of the laser. Normalizing the axial position signal with reference to the instantaneous incident laser power, therefore, provides a significant improvement in the signal-to-noise ratio. The two-dimensional position calibration of the instrument, obtained by raster scanning a stuck bead, is shown in Fig. 7. Stiffness in the lateral dimension was measured by a combination of rolloff, triangle-wave drag force, and variance measurements. Stiffness in the axial dimension was measured using the rolloff method and was found to be ~eightfold less than the lateral stiffness.

Single-molecule transcription experiments were carried out with an RNA polymerase specifically attached to the beads and tethered to the surface of the trapping chamber via one end of the template DNA (Fig. 12). Tethered beads were trapped, the surface position was determined as described above, and the bead was centered over the attachment point of the DNA tether, at a predetermined height. Once these initial conditions were established, the two-dimensional

force-clamp routine was begun. The stage was moved in both the axial and lateral directions until the trapped bead was displaced by a predetermined distance from its equilibrium position. Position signals were recorded at 2 kHz and boxcar averaged over 40 points to generate a 50 Hz signal that was used to control the motion of the stage. In this fashion, the displacement of the bead in the trap, and hence the optical force, was held constant as the tether length changed by micron-scale distances during RNA polymerase movement over the DNA template. The motion of RNA polymerase on the DNA can be calculated from the motion of the stage (Fig. 14). Periods of constant motion interrupted by pauses of variable duration are readily observed in the single-molecule transcription trace shown in Fig. 14. Pauses as short as 1 s are readily detected (Fig. 14, inset). Positional noise is on the order of 2 nm, while drift is less than 0.2 nm/s.

Two-dimensional stage based force clamping affords a unique advantage. Since the stiffness in both dimensions is known, the force vector on the bead is defined and constant during an experiment. Tension in the DNA tether opposes the force on the bead, therefore the angle of the DNA with respect to the surface of the trapping chamber is similarly defined and constant. More importantly, the change in the DNA tether length can be calculated from the motion of the stage in one dimension and the angle calculated from the force in both dimensions. As a result, such measurements are insensitive to drift in the axial dimension, which is otherwise a significant source of instrumental error.

VI. PROGRESS AND OVERVIEW OF OPTICAL TRAPPING THEORY

Optical trapping of dielectric particles is sufficiently complex and influenced by subtle, difficult-to-quantify optical properties that theoretical calculations may never replace direct calibration. That said, recent theoretical work has made significant progress towards a more complete description of optical trapping and three-dimensional position detection based on scattered light. Refined theories permit a more realistic assessment of both the capabilities and the limitations of an optical trapping instrument, and may help to guide future designs and optimizations.

Theoretical expressions for optical forces in the extreme cases of Mie particles ($a \gg \lambda$, a is the sphere radius) and Raleigh particle ($a \ll \lambda$) have been available for some time. Ashkin calculated the forces on a dielectric sphere in the ray-optic regime for both the TEM_{00} and the TEM_{01}^* ("donut mode") intensity profiles.[69] Ray-optics calculations are valid for sphere diameters greater than ~10λ, where optical forces become independent of the size of the sphere. At the other extreme, Chaumet and Nieto-Vesperinas obtained an expression for the total time averaged force on a sphere in the Rayleigh regime[154]

$$\langle F^i \rangle = \left(\frac{1}{2}\right) \text{Re}[\alpha E_{0j} \partial^i (E_0^j)^*], \tag{15}$$

where $\alpha = \alpha_0 (1 - \frac{2}{3} ik^3 \alpha_0)^{-1}$ is a generalized polarizability that includes a damping term, E_0 is the complex magnitude of the electric field, α_0 is the polarizability of a sphere given by Eq.

(4), and k is the wave number of the trapping laser. This expression encapsulates the separate expressions for the scattering and gradient components of the optical force [Eqs. (1) and (3)] and can be applied to the description of optical forces on larger particles through the use of the coupled dipole method.[155] In earlier work, Harada and Asakura calculated the forces on a dielectric sphere illuminated by a moderately focused Gaussian laser beam in the Rayleigh regime by treating the sphere as a simple dipole.[152] The Raleigh theory predicts forces comparable to those calculated with the more complete generalized Lorenz–Mie theory (GLMT) for spheres of diameter up to ~w_0 (the laser beam waist) in the lateral dimension, but only up to ~0.4λ in the axial dimension.[152] More general electrodynamic theories have been applied to solve for the case of spheres of diameter ~λ trapped with tightly focused beams. One approach has been to generalize the Lorenz–Mie theory describing the scattering of a plane wave by a sphere to the case of Gaussian beams. Barton and co-workers applied fifth-order corrections to the fundamental Gaussian beam to derive the incident and scattered fields from a sphere, which enabled the force to be calculated by means of the Maxwell stress tensor.[76,77] An equivalent approach, implemented by Gouesbet and co-workers, expands the incident beam in an infinite series of beam shape parameters from which radiation pressure cross sections can be computed.[80,156] Trapping forces and efficiencies predicted by these theories are found to be in reasonable agreement with experimental values.[157–159] More recently, Rohrbach and co-workers extended the Raleigh theory to larger particles through the inclusion of second-order scattering terms, valid for spheres that introduce a phase shift, $k_0(\Delta n)D$, less than $\pi/3$, where $k_0 = 2\pi/\lambda_0$ is the vacuum wave number, $\Delta n = (n_p - n_m)$ is the difference in refractive index between the particle and the medium, and D is the diameter of the sphere.[65,66] For polystyrene beads ($n_p = 1.57$) in water ($n_m = 1.33$), this amounts to a maximum particle size of ~0.7λ. In this approach, the incident field is expanded in plane waves, which permits the inclusion of apodization and aberration transformations, and the forces are calculated directly from the scattering of the field by the dipole without resorting to the stress tensor approach. Computed forces and trapping efficiencies compare well with those predicted by GLMT,[66] and the effects of spherical aberration have been explored.[65] Since the second-order Raleigh theory calculates the scattered and unscattered waves, the far field interference pattern, which is the basis of the three-dimensional position detection described above, is readily calculated.[63,64]

VII. NOVEL OPTICAL TRAPPING APPROACHES

Optical trapping (OT) has now developed into an active and diverse field of study. Space constraints preclude a complete survey the field, so we have chosen to focus on a small number of recent developments that seem particularly promising for future applications of the technology.

A. Combined optical trapping and single-molecule fluorescence

Combining the complementary techniques of OT and single-molecule fluorescence (SMF) presents significant technological challenges. Difficulties arise from the roughly 15 orders of magnitude difference between the enormous flux of infrared light associated with a typical trapping laser (sufficient to bleach many varieties of fluorescent dye through multiphoton excitation) compared to the miniscule flux of visible light emitted by a single excited fluorophore. These challenges have been met in a number of different ways. Funatsu and co-workers built an apparatus in which the two techniques were employed sequentially, but not simultaneously.[160] In a separate development, Ishijima and co-workers were able to trap beads attached to the ends of a long ($5-10$ μm) actin filament while simultaneously monitoring the binding of fluorescent Adenosine triphosphate (ATP) molecules to a myosin motor interacting with the actin filament.[161] In this way, the coordination between the binding of ATP to myosin and the mechanical motion of the actin filament (detected via the optical trap) was determined. This experiment demonstrated the possibility of simultaneous—but not spatially coincident—OT and SMF in the same microscope field of view. In a more recent development, both simultaneous and spatially coincident OT and SMF have been achieved, and used to measure the mechanical forces required to unzip short duplex regions [15 base pair (bp)] of double-stranded DNA.[138] Dye-labeled hybrids were attached via a long (~1000 bp) DNA "handle" to a polystyrene bead at one end (using the $3'$ end of one strand) and to the coverglass surface at the other (using the $5'$ end of the complementary stand). In one experiment, the adjacent terminal ends of the two strands of the DNA hybrid were each labeled with tetramethylrhodamine (TAMRA) molecules. Due to their physical proximity, these dyes self-quenched (the quenching range for TAMRA is ~1 nm). The DNA hybrid was then mechanically disrupted ("unzipped") by applying a force ramp to the bead while the fluorescence signal was monitored. The point of mechanical rupture detected with the optical trap was coincident with a stepwise increase in the fluorescence signal, as the two dyes separated, leaving behind a dye attached by one DNA strand to the coverglass surface, as the partner dye was removed with the DNA strand attached to the bead. Control experiments with fluorescent dyes attached to either, but not both, DNA strands verified that the abrupt mechanical transition was specific for the rupture of the DNA hybrid and not, for example, due to breakage of the linkages holding the DNA to the bead or the coverglass surface.

B. Optical rotation and torque

Trapping transparent microspheres with a focused Gaussian laser beam in TEM$_{00}$ mode produces a rotationally symmetric trap that does not exert torque. However, several methods have been developed to induce the rotation of trapped objects.[20,52,162] Just as the change of linear momentum due to refraction of light leads to the production of force, a change in angular momentum leads to torque. Cir-

cularly polarized light carries spin angular momentum, of course, and propagating optical beams can also be produced that carry significant amounts of orbital angular momentum, e.g., Laguerre–Gaussian modes.[163] Each photon in such a mode carries $(\sigma+l)\hbar$ of angular momentum, where σ represents the spin angular momentum arising from the polarization state of the light and l is the orbital angular momentum carried by the light pattern. The angular momentum conveyed by the circular polarization alone, estimated at ~10 pN nm/s per mW of 1064 nm light, can be significantly augmented through the use of modes that carry even larger amounts of orbital angular momentum.[164] Transfer of both orbital and spin angular momentum to trapped objects has been demonstrated for absorbing particles.[102,165] Transfer of spin angular momentum has been observed for birefringent particles of crushed calcite,[166] and for more uniform microfabricated birefringent objects.[167,168] Friese and co-workers derived the following expression for the torque on a birefringent particle:[166]

$$\tau = \frac{\varepsilon}{2\omega}E_0^2[\{1-\cos(kd(n_0-n_e))\}\sin 2\varphi$$
$$-\sin(kd(n_0-n_e))\cos 2\varphi \sin 2\theta], \qquad (16)$$

where ε is the permittivity, E_0 is the amplitude of the electric field, ω is the angular frequency of the light, φ describes the ellipticity of the light (plane polarized, $\varphi=0$; circularly polarized, $\varphi=\pi/4$), θ represents the angle between the fast axis of the quarter-wave plate producing the elliptically polarized light and the optic axis of the birefringent particle, k is the vacuum wave number $(2\pi/\lambda)$, and n_0 and n_e are the ordinary and extraordinary indices of refraction of the birefringent material, respectively. Theoretically, all the spin angular momentum carried in a circularly polarized laser beam can be transferred to a trapped object when it acts as a perfect half-wave plate, i.e., $\varphi=\pi/4$ and $kd(n_0-n_e)=\pi$. For the case of plane polarized light, there is a restoring torque on the birefringent particle that aligns the fast axis of the particle with the plane of polarization.[166] Rotation of the plane of polarization will induce rotation in a trapped birefringent particle.

Whereas the transfer of optical angular momentum is a conceptually attractive means of applying torque to optically trapped objects, several other techniques have been employed towards the same end. In one scheme, a high order asymmetric mode, created by placing an aperture in the far field of a laser beam, was used to trap red blood cells: these could be made to spin by rotating the aperture.[169] A more sophisticated version of this same technique involves interfering a Laguerre–Gaussian beam with a plane wave beam to produce a spiral beam pattern.[170] By changing the relative phase of the two beams, the pattern can be made to rotate, leading to rotation in an asymmetric trapped object.[48] Alternatively, the interference of two Laguerre–Gaussian beams of opposite helicity (l and $-l$) creates $2l$ beams surrounding the optical axis, which can be rotated by adjusting the polarization of one of the interfering beams.[46] Additionally, a variety of small chiral objects, such as microfabricated "optical propellers," can be trapped and made to rotate in a symmet-

ric Gaussian beam due to the optical forces generated on asymmetrically oriented surfaces.[171–174]

Rotation of trapped particles is most commonly monitored by video tracking, which is effectively limited by frame rates to rotation speeds below ~15 Hz, and to visibly asymmetric particles (i.e., microscopic objects of sufficient size and contrast to appear asymmetric in the imaging modality used). Rotation rates up to 1 kHz have been measured by back focal plane detection of trapped 0.83 μm beads sparsely labeled with 0.22 μm beads to make these optically anisotropic.[175] Backscattered light from trapped, asymmetric particles has also been used to measure rotation rates in excess of 300 Hz.[102,166]

C. Holographic optical traps

Holograms and other types of diffractive optics have been used extensively for generating complex, high-order optical trapping beams,[20,52,162,165,176] such as the Laguerre–Gaussian modes discussed above. Diffractive optical devices may also be used to synthesize multiple optical traps with arbitrary intensity profiles.[20,91,177–179] A diffractive element placed in a plane optically conjugate to the back aperture of the microscope objective produces an intensity distribution in the specimen plane that is the Fourier transform of the pattern imposed by the element,[177] and several computational methods have been developed to derive the holographic pattern required for any given intensity distribution in the specimen plane.[91,92,180] Generally speaking, diffractive elements modulate both the amplitude and the phase of the incident light. Optical throughput can be maximized by employing diffractive optics that primarily modify the phase but not the amplitude of the incident light, termed kinoforms.[91] Computer-generated phase masks can also be etched onto a glass substrate using standard photolithographic techniques, producing arbitrary, but fixed, optical traps.

Reicherter and co-workers extended the usefulness of holographic optical trapping techniques by generating three independently movable donut-mode trapping beams with an addressable liquid crystal spatial light modulator (SLM).[181] Improvements in SLM technology and real-time hologram calculation algorithms have been implemented, allowing the creation of an array of up to 400 optical traps, in addition to the creation and three-dimensional manipulation of multiple, high order, trapping beams.[92,182,183] Multiple optical traps can also be generated by time sharing, using rapid-scanning techniques based on AODs or galvo mirrors,[49,50] but these are typically formed in just one or two axial planes,[184] and they are limited in number. Dynamic holographic optical tweezers can produce still more varied patterns, limited only by the optical characteristics of the SLM and the computational time required to generate the hologram. Currently, the practical update rate of a typical SLM is around 5 Hz, which limits how quickly objects can be translated.[92] Furthermore, the number and size of the pixels in the SLM restrict the complexity and the range of motion of generated optical traps,[92] while the pixelation and discrete phase steps of the SLM result in diffractive losses. Faster refresh rates (>30 Hz) in a holographic optical trap have recently been reported with a SLM based on ferroelectric, as opposed to

nematic, materials.[185] Further improvements in SLM technology should expand the possible applications of dynamic, holographic optical traps.

VIII. PROSPECTS

The nearly 2 decades that have passed since Ashkin and co-workers invented the single beam, gradient force optical trap have borne witness to a proliferation of innovations and applications. The full potential of most of the more recent optical developments has yet to be realized. On the biological front, the marriage of optical trapping with single-molecule fluorescence methods[138] represents an exciting frontier with enormous potential. Thanks to steady improvements in optical trap stability and photodetector sensitivity, the practical limit for position measurements is now comparable to the distance subtended by a single base pair along DNA, 3.4 Å. Improved spatiotemporal resolution is now permitting direct observations of molecular-scale motions in individual nucleic acid enzymes, such as polymerases, helicases, and nucleases.[86,87,186] The application of optical torque offers the ability to study rotary motors, such as F_1F_0 ATPase,[187] using rotational analogs of many of the same techniques already applied to the study of linear motors, i.e., torque clamps and rotation clamps.[50] Moving up in scale, the ability to generate and manipulate a myriad of optical traps dynamically using holographic tweezers[20,92] opens up many potential applications, including cell sorting and other types of high-throughput manipulation. More generally, as the field matures, optical trapping instruments should no longer be confined to labs that build their own custom apparatus, a change that should be driven by the increasing availability of sophisticated, versatile commercial systems. The physics of optical trapping will continue to be explored in its own right, and optical traps will be increasingly employed to study physical, as well as biological, phenomena. In one ground-breaking example from the field of nonequilibrium statistical mechanics, Jarzynski's equality[188]—which relates the value of the equilibrium free energy for a transition in a system to a *nonequilibrium* measure of the work performed—was put to experimental test by mechanically unfolding RNA structures using optical forces.[189] Optical trapping techniques are increasingly being used in condensed matter physics to study the behavior (including anomalous diffusive properties and excluded volume effects) of colloids and suspensions,[21] and dynamic optical tweezers are particularly well suited for the creation and evolution of large arrays of colloids in well-defined potentials.[20] As optical trapping techniques continue to improve and become better established, these should pave the way for some great new science in the 21st century, and we will be further indebted to the genius of Ashkin.[3]

ACKNOWLEDGMENTS

[1] A. Ashkin, Phys. Rev. Lett. **24**, 156 (1970).
[2] A. Ashkin and J. M. Dziedzic, Appl. Phys. Lett. **19**, 283 (1971).
[3] A. Ashkin et al., Opt. Lett. **11**, 288 (1986).
[4] A. Ashkin, IEEE J. Sel. Top. Quantum Electron. **6**, 841 (2000).
[5] S. Chu et al., Phys. Rev. Lett. **57**, 314 (1986).
[6] A. Ashkin, J. M. Dziedzic, and T. Yamane, Nature (London) **330**, 769 (1987).
[7] A. Ashkin and J. M. Dziedzic, Science **235**, 1517 (1987).
[8] M. J. Lang and S. M. Block, Am. J. Phys. **71**, 201 (2003).
[9] K. Svoboda and S. M. Block, Annu. Rev. Biophys. Biomol. Struct. **23**, 247 (1994).
[10] A. D. Mehta, J. T. Finer, and J. A. Spudich, Methods Enzymol. **298**, 436 (1998).
[11] A. D. Mehta et al., Science **283**, 1689 (1999).
[12] S. C. Kuo, Traffic **2**, 757 (2001).
[13] A. Ishijima and T. Yanagida, Trends Biochem. Sci. **26**, 438 (2001).
[14] Y. Ishii, A. Ishijima, and T. Yanagida, Trends Biotechnol. **19**, 211 (2001).
[15] S. Jeney, E. L. Florin, and J. K. Horber, Methods Mol. Biol. **164**, 91 (2001).
[16] S. Khan and M. P. Sheetz, Annu. Rev. Biochem. **66**, 785 (1997).
[17] R. Simmons, Curr. Biol. **6**, 392 (1996).
[18] C. Bustamante, J. C. Macosko, and G. J. Wuite, Nat. Rev. Mol. Cell Biol. **1**, 130 (2000).
[19] M. D. Wang, Curr. Opin. Biotechnol. **10**, 81 (1999).
[20] D. G. Grier, Nature (London) **424**, 810 (2003).
[21] D. G. Grier, Curr. Opin. Colloid Interface Sci. **2**, 264 (1997).
[22] J. K. H. Horber, *Atomic Force Microscopy in Cell Biology* (Academic, San Diego, 2002), pp. 1–31.
[23] H. Lowen, J. Phys.: Condens. Matter **13**, R415 (2001).
[24] R. Bar-Ziv, E. Moses, and P. Nelson, Biophys. J. **75**, 294 (1998).
[25] P. T. Korda, M. B. Taylor, and D. G. Grier, Phys. Rev. Lett. **89**, 128301 (2002).
[26] L. A. Hough and H. D. Ou-Yang, Phys. Rev. E **65**, 021906 (2002).
[27] B. H. Lin, J. Yu, and S. A. Rice, Phys. Rev. E **62**, 3909 (2000).
[28] J. C. Crocker and D. G. Grier, Phys. Rev. Lett. **77**, 1897 (1996).
[29] J. C. Crocker and D. G. Grier, Phys. Rev. Lett. **73**, 352 (1994).
[30] C. Bustamante, Z. Bryant, and S. B. Smith, Nature (London) **421**, 423 (2003).
[31] C. Bustamante et al., Curr. Opin. Struct. Biol. **10**, 279 (2000).
[32] L. H. Pope, M. L. Bennink, and J. Greve, J. Muscle Res. Cell Motil. **23**, 397 (2002).
[33] J. F. Allemand, D. Bensimon, and V. Croquette, Curr. Opin. Struct. Biol. **13**, 266 (2003).
[34] A. Janshoff et al., Angew. Chem., Int. Ed. **39**, 3213 (2000).
[35] B. Onoa et al., Science **299**, 1892 (2003).
[36] J. Liphardt et al., Science **292**, 733 (2001).
[37] Z. Bryant et al., Nature (London) **424**, 338 (2003).
[38] S. B. Smith, Y. J. Cui, and C. Bustamante, Science **271**, 795 (1996).
[39] M. D. Wang et al., Biophys. J. **72**, 1335 (1997).
[40] T. T. Perkins et al., Science **264**, 822 (1994).
[41] T. T. Perkins, D. E. Smith, and S. Chu, Science **264**, 819 (1994).
[42] T. T. Perkins et al., Science **268**, 83 (1995).
[43] K. Wang, J. G. Forbes, and A. J. Jin, Prog. Biophys. Mol. Biol. **77**, 1 (2001).
[44] A. Ashkin, Proc. Natl. Acad. Sci. U.S.A. **94**, 4853 (1997).
[45] D. McGloin, V. Garces-Chavez, and K. Dholakia, Opt. Lett. **28**, 657 (2003).
[46] M. P. MacDonald et al., Science **296**, 1101 (2002).
[47] V. Garces-Chavez et al., Nature (London) **419**, 145 (2002).
[48] L. Paterson et al., Science **292**, 912 (2001).
[49] K. Visscher, S. P. Gross, and S. M. Block, IEEE J. Sel. Top. Quantum Electron. **2**, 1066 (1996).
[50] K. Visscher and S. M. Block, Methods Enzymol. **298**, 460 (1998).
[51] J. E. Molloy, Methods Cell Biol. **55**, 205 (1998).
[52] J. E. Molloy and M. J. Padgett, Contemp. Phys. **43**, 241 (2002).
[53] G. J. Brouhard, H. T. Schek III, and A. J. Hunt, IEEE Trans. Biomed. Eng. **50**, 121 (2003).

[54] M. P. Sheetz, *in Laser Tweezers in Cell Biology. Methods in Cell Biology*, edited by L. Wilson and P. Matsudaira (Academic, San Diego, 1998), Vol. 55.

[55] S. M. Block, in *Noninvasive Techniques in Cell Biology*, edited by J. K. Foskett and S. Grinstein (Wiley-Liss, New York, 1990), pp. 375–402.

[56] S. E. Rice, T. J. Purcell, and J. A. Spudich, Methods Enzymol. **361**, 112 (2003).

[57] S. B. Smith, Y. Cui, and C. Bustamante, Methods Enzymol. **361**, 134 (2003).

[58] S. M. Block, in *Constructing Optical Tweezers, Cell Biology: A Laboratory Manual*, edited by D. Spector, R. Goldman, and L. Leinward (Cold Spring Harbor Press, Cold Spring Harbor, NY, 1998).

[59] M. J. Lang *et al.*, Biophys. J. **83**, 491 (2002).

[60] E. Fallman and O. Axner, Appl. Opt. **36**, 2107 (1997).

[61] E. J. G. Peterman *et al.*, Rev. Sci. Instrum. **74**, 3246 (2003).

[62] A. Pralle *et al.*, Microsc. Res. Tech. **44**, 378 (1999).

[63] A. Rohrbach, H. Kress, and E. H. Stelzer, Opt. Lett. **28**, 411 (2003).

[64] A. Rohrbach and E. H. K. Stelzer, J. Appl. Phys. **91**, 5474 (2002).

[65] A. Rohrbach and E. H. Stelzer, Appl. Opt. **41**, 2494 (2002).

[66] A. Rohrbach and E. H. Stelzer, J. Opt. Soc. Am. A Opt. Image Sci. Vis **18**, 839, (2001).

[67] J. D. Jackson, *Classical Electrodynamics*, 2nd ed. (Wiley, New York, 1975).

[68] A. Ashkin, *Methods in Cell Biology* (Academic, San Diego, 1998), Vol. 55, pp. 1–27.

[69] A. Ashkin, Biophys. J. **61**, 569 (1992).

[70] E. Fallman and O. Axner, Appl. Opt. **42**, 3915 (2003).

[71] A. T. O'Neill and M. J. Padgett, Opt. Commun. **193**, 45 (2001).

[72] N. B. Simpson *et al.*, J. Mod. Opt. **45**, 1943 (1998).

[73] M. E. J. Friese *et al.*, Appl. Opt. **35**, 7112 (1996).

[74] E. Almaas and I. Brevik, J. Opt. Soc. Am. B **12**, 2429 (1995).

[75] J. P. Barton, J. Appl. Phys. **64**, 1632 (1988).

[76] J. P. Barton and D. R. Alexander, J. Appl. Phys. **66**, 2800 (1989).

[77] J. P. Barton, D. R. Alexander, and S. A. Schaub, J. Appl. Phys. **66**, 4594 (1989).

[78] P. Zemanek, A. Jonas, and M. Liska, J. Opt. Soc. Am. A Opt. Image Sci. Vis **19**, 1025 (2002).

[79] G. Gouesbet and G. Grehan, Atomization Sprays **10**, 277 (2000).

[80] K. F. Ren, G. Greha, and G. Gouesbet, Opt. Commun. **108**, 343 (1994).

[81] K. Visscher, M. J. Schnitzer, and S. M. Block, Nature (London) **400**, 184 (1999).

[82] M. D. Wang *et al.*, Science **282**, 902 (1998).

[83] G. J. Wuite *et al.*, Nature (London) **404**, 103 (2000).

[84] R. S. Rock *et al.*, Proc. Natl. Acad. Sci. U.S.A. **98**, 13655 (2001).

[85] S. M. Block *et al.*, Proc. Natl. Acad. Sci. U.S.A. **100**, 2351 (2003).

[86] T. T. Perkins *et al.*, Science **301**, 1914 (2003).

[87] K. C. Neuman *et al.*, Cell **115**, 437 (2003).

[88] K. Adelman *et al.*, Proc. Natl. Acad. Sci. U.S.A. **99**, 13538 (2002).

[89] <http://www.cellrobotics.com>

[90] <http://www.arryx.com/home1.html>

[91] E. R. Dufresne *et al.*, Rev. Sci. Instrum. **72**, 1810 (2001).

[92] J. E. Curtis, B. A. Koss, and D. G. Grier, Opt. Commun. **207**, 169 (2002).

[93] <http://www.palm-mikrolaser.com>

[94] S. P. Gross, Methods Enzymol. **361**, 162 (2003).

[95] K. C. Neuman *et al.*, Biophys. J. **77**, 2856 (1999).

[96] H. Liang *et al.*, Biophys. J. **70**, 1529 (1996).

[97] I. A. Vorobjev *et al.*, Biophys. J. **64**, 533 (1993).

[98] A. Ashkin and J. M. Dziedzic, Ber. Bunsenges. Phys. Chem. Chem. Phys. **93**, 254 (1989).

[99] Y. Liu *et al.*, Biophys. J. **68**, 2137 (1995).

[100] E. J. G. Peterman, F. Gittes, and C. F. Schmidt, Biophys. J. **84**, 1308 (2003).

[101] A. Schonle and S. W. Hell, Opt. Lett. **23**, 325 (1998).

[102] M. E. J. Friese *et al.*, Phys. Rev. A **54**, 1593 (1996).

[103] G. J. Wuite *et al.*, Biophys. J. **79**, 1155 (2000).

[104] W. Grange *et al.*, Rev. Sci. Instrum. **73**, 2308 (2002).

[105] S. Inoue and K. R. Spring, *Video Microscopy: The Fundamentals*, 2nd ed. (Plenum, New York, 1997).

[106] H. Misawa *et al.*, J. Appl. Phys. **70**, 3829 (1991).

[107] S. C. Kuo and J. L. McGrath, Nature (London) **407**, 1026 (2000).

[108] Y. L. Kuo *et al.*, Arch. Androl **44**, 29 (2000).

[109] S. Yamada, D. Wirtz, and S. C. Kuo, Biophys. J. **78**, 1736 (2000).

[110] M. K. Cheezum, W. F. Walker, and W. H. Guilford, Biophys. J. **81**, 2378 (2001).

[111] R. E. Thompson, D. R. Larson, and W. W. Webb, Biophys. J. **82**, 2775 (2002).

[112] J. C. Crocker and D. G. Grier, J. Colloid Interface Sci. **179**, 298 (1996).

[113] C. Gosse and V. Croquette, Biophys. J. **82**, 3314 (2002).

[114] M. Keller, J. Schilling, and E. Sackmann, Rev. Sci. Instrum. **72**, 3626 (2001).

[115] V. Croquette (personal communication).

[116] J. T. Finer, R. M. Simmons, and J. A. Spudich, Nature (London) **368**, 113 (1994).

[117] J. E. Molloy *et al.*, Biophys. J. **68**, S298 (1995).

[118] W. Denk and W. W. Webb, Appl. Opt. **29**, 2382 (1990).

[119] K. Svoboda *et al.*, Nature (London) **365**, 721 (1993).

[120] F. Gittes and C. F. Schmidt, Opt. Lett. **23**, 7 (1998).

[121] F. Gittes and C. F. Schmidt, Biophys. J. **74**, A183 (1998).

[122] M. W. Allersma *et al.*, Biophys. J. **74**, 1074 (1998).

[123] L. P. Ghislain and W. W. Webb, Opt. Lett. **18**, 1678 (1993).

[124] L. P. Ghislain, N. A. Switz, and W. W. Webb, Rev. Sci. Instrum. **65**, 2762 (1994).

[125] I. M. Peters *et al.*, Rev. Sci. Instrum. **69**, 2762 (1998).

[126] M. E. J. Friese *et al.*, Appl. Opt. **38**, 6597 (1999).

[127] E. L. Florin *et al.*, J. Struct. Biol. **119**, 202 (1997).

[128] E. L. Florin, J. K. H. Horber, and E. H. K. Stelzer, Appl. Phys. Lett. **69**, 446 (1996).

[129] Z. X. Zhang *et al.*, Appl. Opt. **37**, 2766 (1998).

[130] A. Jonas, P. Zemanek, and E. L. Florin, Opt. Lett. **26**, 1466 (2001).

[131] K. Sasaki, M. Tsukima, and H. Masuhara, Appl. Phys. Lett. **71**, 37 (1997).

[132] A. R. Clapp, A. G. Ruta, and R. B. Dickinson, Rev. Sci. Instrum. **70**, 2627 (1999).

[133] A. E. Siegman, Lasers University Science Books (Sausalito, CA, 1986), p. 1283.

[134] K. Berg-Sorensen *et al.*, J. Appl. Phys. **93**, 3167 (2003).

[135] S. J. Koch and M. D. Wang, Phys. Rev. Lett. **91**, 028103 (2003).

[136] B. D. Brower-Toland *et al.*, Proc. Natl. Acad. Sci. U.S.A. **99**, 1960 (2002).

[137] S. J. Koch *et al.*, Biophys. J. **83**, 1098 (2002).

[138] M. J. Lang, P. M. Fordyce, and S. M. Block, J. Biol. **2**, 6 (2003).

[139] T. D. Visser and S. H. Wiersma, J. Opt. Soc. Am. A Opt. Image Sci. Vis **9**, 2034 (1992).

[140] S. H. Wiersma *et al.*, J. Opt. Soc. Am. A Opt. Image Sci. Vis **14**, 1482 (1997).

[141] S. H. Wiersma and T. D. Visser, J. Opt. Soc. Am. A Opt. Image Sci. Vis **13**, 320 (1996).

[142] K. Carlsson, J. Microsc. **163**, 167 (1991).

[143] P. Bartlett, S. I. Henderson, and S. J. Mitchell, Philos. Trans. R. Soc. London, Ser. A **359**, 883 (2001).

[144] S. Hell *et al.*, J. Microsc. **169**, 391 (1993).

[145] J. Radler and E. Sackmann, Langmuir **8**, 848 (1992).

[146] K. C. Neuman, E. A. Abbondanzieri, and S. M. Block (unpublished).

[147] H. Brenner, Chem. Eng. Sci. **16**, 242 (1961).

[148] K. Berg-Sørensen and H. Flyvbjerg, Rev. Sci. Instrum. **75**, 594 (2004).

[149] I. M. Toliæ-Nørrelykke, K. Berg-Sørensen, and H. Flyvbjerg, Comput. Phys. Commun. **159**, 225 (2004).

[150] T. R. Strick *et al.*, Biophys. J. **74**, 2016 (1998).

[151] T. R. Strick *et al.*, Science **271**, 1835 (1996).

[152] Y. Harada and T. Asakura, Opt. Commun. **124**, 529 (1996).

[153] K. Svoboda and S. M. Block, Cell **77**, 773 (1994).

[154] P. C. Chaumet and M. Nieto-Vesperinas, Opt. Lett. **25**, 1065 (2000).

[155] P. C. Chaumet and M. Nieto–Vesperinas, Phys. Rev. B **61**, 4119 (2000).

[156] G. Gouesbet, B. Maheu, and G. Grehan, J. Opt. Soc. Am. A Opt. Image Sci. Vis **5**, 1427 (1988).

[157] Y. K. Nahmias and D. J. Odde, Int. J. Quantum Chem. **38**, 131 (2002).

[158] W. H. Wright, G. J. Sonek, and M. W. Berns, Appl. Opt. **33**, 1735 (1994).

[159] W. H. Wright, G. J. Sonek, and M. W. Berns, Appl. Phys. Lett. **63**, 715 (1993).

[160] T. Funatsu *et al.*, Biophys. Chem. **68**, 63 (1997).

[161] A. Ishijima *et al.*, Cell **92**, 161 (1998).

[162] K. Dholakia, G. Spalding, and M. MacDonald, Phys. World **15**, 31 (2002).

[163] S. M. Barnett and L. Allen, Opt. Commun. **110**, 670 (1994).

[164] L. Allen *et al.*, Phys. Rev. A **45**, 8185 (1992).

[165] H. He *et al.*, Phys. Rev. Lett. **75**, 826 (1995).

[166] M. E. J. Friese *et al.*, Nature (London) **394**, 348 (1998).

[167] E. Higurashi, R. Sawada, and T. Ito, J. Micromech. Microeng. **11**, 140 (2001).

[168] E. Higurashi, R. Sawada, and T. Ito, Phys. Rev. E **59**, 3676 (1999).

[169] S. Sato, M. Ishigure, and H. Inaba, Electron. Lett. **27**, 1831 (1991).

[170] M. Padgett et al., Am. J. Phys. **64**, 77 (1996).

[171] E. Higurashi et al., Appl. Phys. Lett. **64**, 2209 (1994).

[172] E. Higurashi et al., J. Appl. Phys. **82**, 2773 (1997).

[173] R. C. Gauthier, Appl. Phys. Lett. **67**, 2269 (1995).

[174] R. C. Gauthier, Appl. Opt. **40**, 1961 (2001).

[175] A. D. Rowe et al., J. Mod. Opt. **50**, 1539 (2003).

[176] H. He, N. R. Heckenberg, and H. Rubinsztein-Dunlop, J. Mod. Opt. **42**, 217 (1995).

[177] E. R. Dufresne and D. G. Grier, Rev. Sci. Instrum. **69**, 1974 (1998).

[178] P. Korda et al., Rev. Sci. Instrum. **73**, 1956 (2002).

[179] D. M. Mueth et al., Phys. Rev. Lett. **77**, 578 (1996).

[180] J. Liesener et al., Opt. Commun. **185**, 77 (2000).

[181] M. Reicherter et al., Opt. Lett. **24**, 608 (1999).

[182] J. E. Curtis and D. G. Grier, Opt. Lett. **28**, 872 (2003).

[183] Y. Igasaki et al., Opt. Rev. **6**, 339 (1999).

[184] A. van Blaaderen et al., Faraday Discuss. **123**, 107 (2003).

[185] W. J. Hossack et al., Opt. Express **11**, 2053 (2003).

[186] J. W. Shaevitz et al., Nature (London) **426**, 684 (2003).

[187] H. Noji et al., Nature (London) **386**, 299 (1997).

[188] C. Jarzynski, Phys. Rev. Lett. **78**, 2690 (1997).

[189] J. Liphardt et al., Science **296**, 1832 (2002).